Ionospheric errors in GPS

Measuring and modelling the ionospheric delay using single and dual frequency receivers

K.A. Beenen

This project has received funding from the European Union's Horizon 2020 Research and Innovation Programme under grant agreement No.776691. The opinions expressed in this report are of the authors only and no way reflect the European Commission's opinions. The European Union is not liable for any use that may be made of the information.

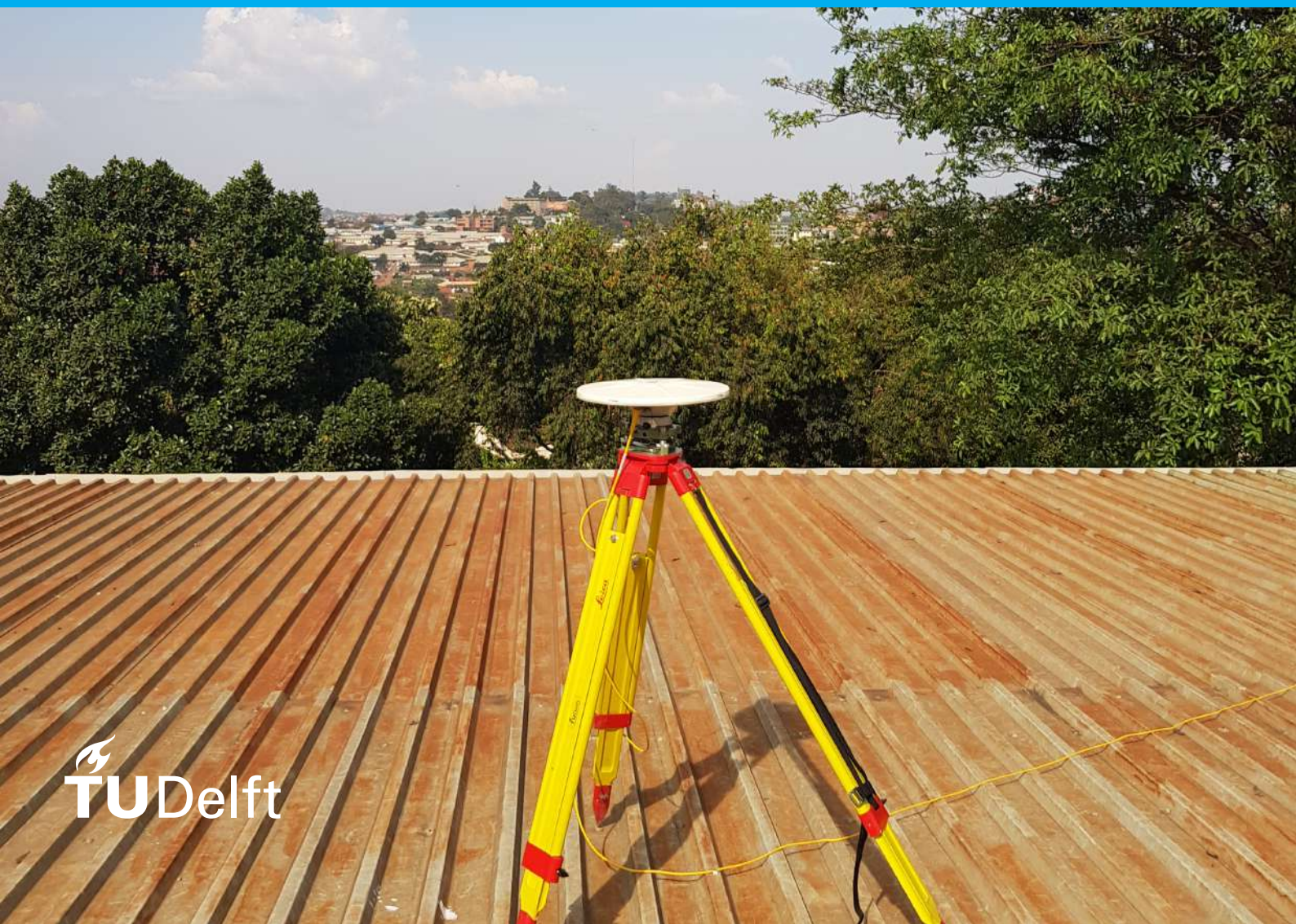

TU Delft

Ionospheric errors in GPS

Measuring and modelling the ionospheric delay using single and dual frequency receivers

by

K.A. Beenen

in partial fulfilment of the requirements for the degree of
Master of Science
in Applied Earth Sciences
at the Delft University of Technology,

Student number: 4139984

Supervisors:	Prof. Dr. ir. Nick van de Giesen	TU Delft
	Dr. ir. Sandra Verhagen	TU Delft
	Assoc. Prof. Dr. Florence D'ujanga,	Makerere University

TU Delft

TWIGA

Preface

This additional thesis is written as part of my master degree in “Geoscience and Remote Sensing” at the Delft University of Technology. In this study the measurements are obtained in Uganda.

In the second year of the master studies students have the opportunity to do some free electives. I choose to do an additional thesis as a free elective instead of courses. The main reason for doing this is to gain more experience in fieldwork, scientific thinking and writing. Also it gives me the chance to do an research abroad and to experience living in another country and culture. For the additional thesis a feasibility study is done using a network of single and dual frequency receivers to monitor and estimate the ionospheric delay in Uganda. In this report the theory used, the designed network and obtained results will be analysed.

I would like to thank Nick van de Giesen and Florence d’Ujanga for giving us the opportunity to do this project in Kampala, Uganda. I would like to thank Sandra Verhagen for being my supervisor from Geoscience and Remote Sensing. Moreover, I would like to thank Andreas Krietemeyer for helping me obtaining and installing the single frequency receivers and that he is always available for any question I had about GPS. In addition, I would like to thank Richard Cliffe for making time to find secure locations for setting up the GPS receivers and getting me in contact with the schools. Furthermore, I would like to thank Hans van der Marel for loaning out the dual receivers.

Kathelijne Beenen
Delft, January 2020

Contents

Preface ii

Abstract v

1 Introduction 1
- 1.1 Research relevance . . . 1
- 1.2 Research motivation . . . 2
- 1.3 Research objective and questions . . . 2
- 1.4 Report outline . . . 2

2 Background information GPS 3
- 2.1 Measurements in GPS . . . 3
  - 2.1.1 Code phase measurements . . . 3
  - 2.1.2 Carrier phase measurements . . . 4
- 2.2 Errors sources . . . 4
  - 2.2.1 Errors at the satellite . . . 4
  - 2.2.2 Errors at the receiver . . . 4
  - 2.2.3 Atmospheric errors . . . 5

3 Determining ionospheric delay 9
- 3.1 Equipment . . . 9
  - 3.1.1 Dual frequency receivers . . . 9
  - 3.1.2 Single frequency receivers . . . 9
- 3.2 SEID model . . . 9
- 3.3 Further processing of data: Precise point positioning (PPP) . . . 11

4 Network set-up 12
- 4.1 Ideal network . . . 12
- 4.2 Network set-up Uganda . . . 12
  - 4.2.1 Network set-up round 1 . . . 13
  - 4.2.2 Network set-up round 2 . . . 15

5 Results & discussion 18
- 5.1 Ionospheric delay of the dual frequency receivers . . . 18
- 5.2 Epoch-difference ionospheric delay . . . 21
- 5.3 Ionospheric delay of the single frequency receivers . . . 22
- 5.4 Total electron content . . . 25

6 Conclusion 26

7 Recommendations 28
- 7.1 Network set-up . . . 28
- 7.2 Data . . . 28
- 7.3 Data processing . . . 29
- 7.4 U-blox Dual frequency receivers . . . 29
- 7.5 Other models . . . 29

Bibliography 30

Appendices 32

A Data conversion 33
- A.1 Dual frequency . . . 33
- A.2 Single frequency . . . 33

B Ionospheric delay Buloba dual frequency receiver **34**

C Epoch-difference ionospheric delay **36**

Abstract

Accurate weather forecasting plays an important role in predicting precipitation events. With the warming climate the precipitable water vapour in the atmospheric is increasing. Since weather parameters as precipitable water vapor have a high spatial variability, interpolation of water vapor data over an area of hundreds of kilometer does not have a sufficient quality for weather prediction applications. Nowadays, researchers are investigating if the precipitable water vapour can be quantified using GPS transmitted signals in a densified GPS network. An accurate quantification of the ionospheric delay is important to efficiently calculate the precipitable water vapour. Moreover, the ionospheric delay is the biggest error and limitation of the GPS signal. It is important to understand how the ionospheric delay varies spatially and in time. Therefore, variability in the ionospheric delay is an interesting factor in weather forecasting and climate change.

To monitor the ionospheric delay a high temporal (in minutes) and spatial resolution (in km-grid) is needed, because the ionospheric delay changes spatially and throughout the day. A possibility to achieve this is to densify GPS networks. Previous research has shown that it is possible to measure the ionospheric delay with dual frequency receivers. In developing countries this densification of GPS networks cannot be achieved with expensive dual-frequency receivers. This study investigates if a higher receiver network density can be achieved with the help of low-cost single frequency receivers. Therefore, a densified GPS network of dual and single frequency receivers is set-up in and around Kampala, Uganda.

This research demonstrates how the Satellite-specific Epoch-difference Ionospheric Delay model (SEID) can be used to compute the ionospheric delay for a single frequency receiver through time. The SEID model creates a second frequency for a single frequency receiver which is used to resolve the ionospheric delay. The intensity of the ionospheric delay depends on the electrons in the ionosphere. The number of free electrons in the path of a signal is expressed as the total electron content. This research shows how to compute the total electron content in the ionospheric layer of the atmosphere. After computing the second frequency for the single frequency receivers the observations need to be processed using Precise Point Positioning (PPP) to compute the precipitable water vapour. As a case study Uganda is chosen, because it is located on the equator. The ionospheric delay fluctuates more at the equator so this is an interesting region to investigate the variability.

The analysis shows that an high accuracy of the GPS signal is needed to create desirable results. Therefore, field campaigns with single frequency and dual frequency receivers should incorporate antennas with noise reduction. In order tot assess the accuracy of the ionospheric delay obtained by using single and dual frequency receivers, future research should be focus on better network set-up and getting the right equipment with better noise reduction.

Keywords: GPS, SEID model, Ionospheric delay, single frequency receivers

1 Introduction

This additional thesis is part of the TWIGA project (Transforming water, weather, and climate information through in situ observations for geo-sevices in Africa) [TWIGA, 2020, TU Delft, 2017]. The aim of the TWIGA project is to provide geo-information on weather, water, and climate in Africa through in-situ measurements and satellite data [TU Delft, 2017]. The goal of this research project is to get more accurate weather prediction by using a network of dual and single frequency GPS (Global Positioning System) receivers. The TWIGA project is funded under the EU H2020 and on the website of TWIGA it is stated that:

This project has received funding from the European Union's Horizon 2020 Research and Innovation Programme under grant agreement No.776691. The opinions expressed in this report are of the authors only and no way reflect the European Commission's opinions. The European Union is not liable for any use that may be made of the information.

Figure 1.1: Twiga logo [TWIGA, 2020]

1.1. Research relevance

TWIGA would like to improve the weather and climate information in Africa by using GPS. Since weather parameters such as water vapor have a high spatial variability, interpolation of water vapor data derived by dual frequency GPS receivers does not have a sufficient quality for weather prediction applications [Deng et al., 2012]. Therefore, the GPS networks should be more densified to capture the spatial variability of the weather. For this research a densified GPS network of dual and single frequency receivers is set-up to measure the ionospheric delay in and around Kampala, the capital city of Uganda. Single frequency receivers are used to densify the network because of their low-cost of about a few hundred euros. Moreover, an important aspect of improving weather forecasting is to determine the effect of ionospheric delay. The ionospheric delay is an error source, which is needed to deal with when deriving weather parameters such water vapour content with GPS. Currently, the biggest error source and limitation in the GPS signal of the single frequency receivers is the ionospheric delay [Krietemeyer et al., 2018]. The intensity of the ionospheric delay depends on the geomagnetic conditions, the season, the solar cycle and the time of the day. Furthermore, the ionospheric delay fluctuates more near the equator, which is discussed in more detail in chapter 2. The equator intersects the country of Uganda. Therefore, this country is chosen as the study site.

In this research Satellite-specific and Epoch-differenced Ionospheric Delay (SEID) model is used to compute the ionospheric delay at single frequency receivers, which is introduced by Deng et al. (2009). This additional thesis investigates the feasibility of determining the ionospheric delay using a densified network of single frequency receivers.

1.2. Research motivation

In the past research has be done by TAHMO (Trans-African Hydro-Meteorological Observatory) and by the department of Water Resources at the Delft University of Technology [TAHMO, 2020]. Two students, Mariska Koning and Eva Stierman have set up a temporal network of dual and single frequency receivers to measure the precipitable water vapour and the total tropospheric delay in 2016 in Uganda [Koning, 2017, Stierman, 2017]. The conclusion of this research was that the measurements done by single frequency receivers was not accurate nor precise enough for estimating the zenith tropospheric delay [Koning, 2017, Stierman, 2017]. As an extension on the research of Koning (2017) and Stierman (2017) this research focuses on estimating the ionospheric delay with patched and Tallysman antennas. This is because before computing the total tropospheric delay as well as the precipitable water vapour the ionospheric delay needs to be derived to eliminate this error source. Therefore, Koning (2017) and Stierman (2017) computed the ionospheric delay before computing the precipitable water vapour. However, they did not look at the accuracy of the estimated ionospheric delay. In this study, the Tallysman antennas should ensure a decrease in the multipath error compared to the patched antennas. The assumption is by using antennas with decreasing multipath error a estimation with a higher accuracy of ionosheric delay can be computed. Furthermore, the total electron content will be computed n this study. The total electron content in the ionosphere is in relation with the ionospheric delay. A higher total electron content causes a higher error. This additional thesis has the following purposes:

- Give more insight if the ionospheric delay can be estimated accurately enough.
- Give more insight on the how the ionospheric delay and total electron content vary spatially throughout a day.

1.3. Research objective and questions

During this research it will be investigated how the ionosphere is behaving during a time span of 24 hours at the equator in a rainy season. The main question for this research is :

What accuracy can be obtained for ionospheric delay in Uganda using single and dual frequency receivers and what is the total electron content in the ionosphere?

The main research question is based on the following sub-questions:

- Can the ionospheric delay be estimated with single frequency receivers?
- What is the difference in ionospheric delay between single frequency and dual frequency at the same location?
- How does the ionospheric delay and total electron content spatially vary throughout a day?

1.4. Report outline

Firstly, in this report relevant background information on GPS will be discussed in chapter 2. In chapter 3 an approach to determine the ionospheric delay will be explained. Furthermore, the ideal network set-up and the actual network set-up in Uganda will be described in chapter 4. The results will be analyzed and discussed in chapter 5. At last, the conclusion of this research can be found in chapter 6 and the recommendation can be found in chapter 7.

2

Background information GPS

2.1. Measurements in GPS

The GPS station measures two different signal, namely the code phase and the carrier phase. This section explains the measurements types in more detail.

2.1.1. Code phase measurements

The GPS receivers measure the difference between the time of the signal transmission from the satellite and the time of reception of signal at the receiver. The time of the signal emitted by the satellite is marked in the code of the signal. At the receiver the amount of time shift needed to align the C/A-code replica from the satellite is calculated [Misra and Enge, 2001]. The time shift measurement is biased, since the clocks of the satellite and receiver are not synchronized. The pseudo range is the measured apparent range, which is formulated in equation 2.1 [Misra and Enge, 2001]. The biased pseudo range is defined as the transit time τ, $t^s(t-\tau)$ is the time stamp of the emitted signal from the satellite, see equation 2.2, and $t_u(t)$ is the arrival time of the signal at the receiver, see equation 2.3 [Misra and Enge, 2001]. Furthermore, c indicates the speed of light in a vacuum.

$$\rho(t) = c[t_u(t) - t^s(t-\tau)] \tag{2.1}$$

$$t_u(t) = t + \delta t_u(t) \tag{2.2}$$

$$t^s(t-\tau) = (t-\tau) + \delta t^s(t-\tau) \tag{2.3}$$

In equation 2.2, the receiver clock bias is $\delta t_u(t)$ and in equation 2.3 δt^s is the satellite clock bias. However, besides of clock biases, which occur in the signal, noise and modelling and measurements errors occur in the signal. Thus, the pseudorange measurement is described in equation 2.4 as

$$C(t) = c\tau + c[\delta t_u)\, t) - \delta t^s(t-\tau)] + \eta c(t) \tag{2.4}$$

The distance traveled by the signal is expressed in equation 2.5 as $c\tau$

$$c\tau = r(t, t-\tau) + I + T \tag{2.5}$$

The code measurements can be reformulated as

$$\rho = r + c[\delta t_u - \delta t^s] + I_\rho + T_\rho + \eta_\rho \tag{2.6}$$

where r is the geometric range between receiver at time t and satellite at time $t-\tau$, I_ρ is the ionospheric delay and T_ρ is the tropospheric delay.

2.1.2. Carrier phase measurements

The carrier phase measurements measures the difference between phases of the signal of the receiver generated signal and the received signal. This means it computes how many cycles are needed to shift the received carrier signal to get full correlation with the generated carrier signal. However, keep in mind that carrier phase measurement contains no information about the number of whole cycles, which is referred to as the integer ambiguity [Misra and Enge, 2001].

$$\phi(t) = \phi_u(t) - \phi^s(t-\tau) + N \tag{2.7}$$

In equation 2.7 the phase of the receiver-generated signal is ϕ_u, the phase of the signal received from the satellite at time t is $\phi^s(t-\tau)$ and N is the integer ambiguity [Misra and Enge, 2001].

Like with code phase measurements atmospheric delay, clock errors, measurements and modelling errors occur in the signal, so the carrier phase measurement can be rewritten as:

$$\phi = \lambda^{-1}[r + I_\phi + T_\phi] + \frac{c}{\lambda}(\delta t_u - \delta t^s) + N + \epsilon_\phi \tag{2.8}$$

Here, λ is the wavelength of the signal and can be computed as:

$$\lambda = c/f \tag{2.9}$$

2.2. Errors sources

While doing GPS measurements different kind of errors can occur, which can have a influence on your measurements results. In this section different kind of important errors for this research are explained.

2.2.1. Errors at the satellite

2.2.1.1. Satellite clock error

The atomic clocks in the satellites are very accurate and precise, but they do drift a small amount [Li et al., 2018]. A small inaccuracy in the satellite clock can still influence the position estimated by the receiver significantly [Li et al., 2018]. The satellite clock error is estimated by the control segment and send with a broadcast message [Misra and Enge, 2001].

2.2.1.2. Satellite ephemeris error

The satellite transmits information about the state of the satellite, such as the actual and predicted location of the satellite, velocity and time, which is called the ephemeris data [Misra and Enge, 2001]. The satellite ephemeris error describes the difference between the actual and predicted orbital position of the satellite. The satellite ephemeris error decompose of the following components along the satellite orbit: radial, along-track and across track errors [Misra and Enge, 2001]. A small error in the orbital position can still have a huge influence on the estimated GPS position and reduces the accuracy [Misra and Enge, 2001]. GPS receivers that are able to process ephemerides data can compensate for some of the orbital errors.

For a single frequency receiver the satellite clock and ephemeris error can cause a root mean square range error of approximately 3 meter for pseudorange measurements [Misra and Enge, 2001].

2.2.2. Errors at the receiver

2.2.2.1. Receiver clock error

Like as the satellite clock the receiver clock drifts as well. The deviation from time is limited in the receiver based on the estimated clock error. To compute the receiver clock error at least 4 satellites are needed. By estimating the receiver clock error, the error can be eliminated from the signal. To reduce the receiver clock error continuous clock steering or to reset the clock (clock jump) when a certain threshold is reached.

2.2.2.2. Multipath

When looking at figure 2.1 the GPS signal can be reflected on surrounding objects such as buildings or via the ground to the receiver. When a signal reaches the antenna via two or more path, this is called multipath. The multipath signal is a delayed signal of the direct signal and usually a weaker version of the direct signal (i.e. line of sight) [Misra and Enge, 2001]. Although multipath signals can either interfere with the direct GPS signals or be mistaken for the direct signal [Williams, 2001]. An approach for minimizing multipath errors are to track only those satellites from a certain angle, for example 15 °, above the horizon.

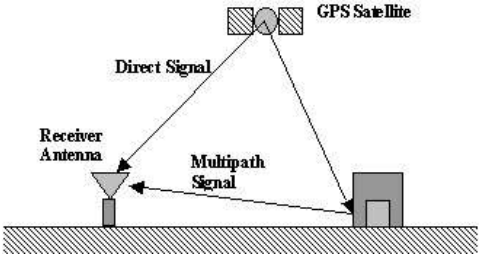

Figure 2.1: Multipath signal [Williams, 2001]

Receiver clock error and the multipath error can cause a root mean square range error of 1 meter for pseudorange measurements for a single frequency receiver [Misra and Enge, 2001]. Furthermore, keep in mind that the multipath error can easily be higher than the assumed range error [Misra and Enge, 2001].

2.2.3. Atmospheric errors

Since the GPS signal travels through the earths atmosphere, changes in the GPS signal occur. Refraction of the GPS signals results in changes in speed and direction of the signal. These changes can be divided in a delay of two atmospheric layers, namely the ionosphere and troposphere. For single frequency receivers the atmospheric error can cause a root mean square range error of approximately 5 meter for pseudorange measurements [Misra and Enge, 2001]. However, the atmospheric error can be double as high in the equatorial region or at high latitudes for a single frequency receiver during high solar activity [Misra and Enge, 2001]. The atmospheric errors are the biggest error source compared to the above mentioned errors at the satellite and the receiver. The error size of ionospheric and troposheric delay differs. The ionospheric delay has a high variability, whereas the error range can change from several meters to several tens of meters [Misra and Enge, 2001]. The tropospheric delay is much lower and less variable, which is at sea level approximately between 2.3-2.6 meter [Misra and Enge, 2001].

2.2.3.1. Ionospheric delay

The ionosphere is an atmospheric layer, which is at a height from 50 km to about 1000 km above the earth [Misra and Enge, 2001]. The ionosphere consists of ionized gases. The delay caused by the ionosphere depends on the electron density in the ionosphere layer. This ionospheric delay caused errors in the GPS positioning, because the speed and direction of the GPS signal changes.

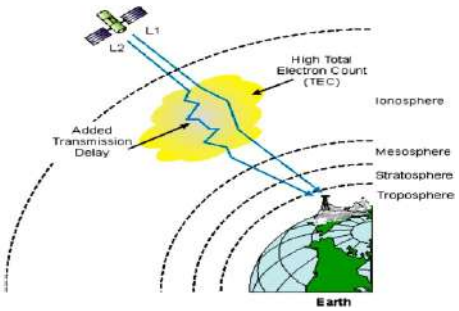

Figure 2.2: Refraction of the GPS signal in the ionosphere [Abba et al., 2015]

The ionization of these gases are caused by solar radiation, however the intensity of the ionization differs in time and space. The intensity of the ionospheric delay depends on the geomagnetic conditions, season, solar cycle and the time of the day. Gas molecules are breaking up into ions and free electrons by ultraviolet radiation transmitted by the sun [Misra and Enge, 2001]. During the night there is no ultraviolet radiation and therefore the electron density reduces. Differences in the electron density between day and night can go up to two orders of magnitude. Furthermore, the solar radiation changes with season, which is visualized in figure 2.4. Also the Sun has a 11-year solar cycle, which causes variation in solar radiation during the cycle and visualized in figure 2.5. All this together causes a variation from day to day in ionospheric delay.

The number of free electrons in the path of signal in the ionosphere is expressed as the total electron content (TEC). The total electron content is defined as the number of electrons in a tube of 1 m^2 cross section extending from the receiver to the satellite and visualized in figure 2.3 [Misra and Enge, 2001].

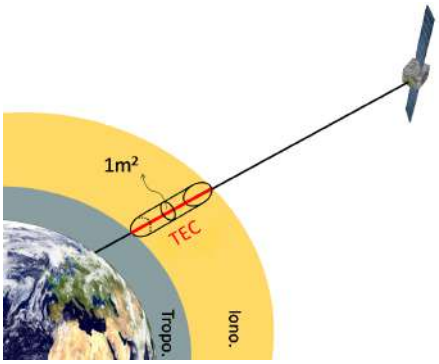

Figure 2.3: Slant Total Electron Content [Royal Observatory of Belgium GNSS Research Group, 2014]

The total electron density can be computed as in equation 2.10.

$$TEC = \int_S^R n_e(l)dl \tag{2.10}$$

In equation 2.10 $n_e(l)$ is the number of free electrons along the signal path and the integration is along the signal path from satellite to receiver [Misra and Enge, 2001]. TEC is measured in TEC units, where 1 TECU is 10^16 electrons/m^2 [Teunissen and Montenbruck, 2017].

The total electron content is in relation with the ionospheric delay according to the ionospheric refraction equation [Royal Observatory of Belgium GNSS Research Group, 2014]. The phase ionospheric delay is a function of the TEC as shown in equation 2.11 [Misra and Enge, 2001].

$$I_\phi = -\frac{40.3 * TEC}{f^2} \tag{2.11}$$

The ionosphere delay terms for pseudorange and carrier phase are equal in magnitude but opposite in sign, see equation 2.12, [Misra and Enge, 2001].

$$I_\rho = -I_\phi = \frac{40.3 * TEC}{f^2} \tag{2.12}$$

Furthermore, the total electron content can be obtained straightly from the pseudo-range measurements, which is formalized in equation 2.13 [Poh and Kamarudin, 2006].

$$TEC = \frac{(R2–R1) - \epsilon_{r21}}{\frac{40.3}{f_2^2} - \frac{40.3}{f_1^2}} \tag{2.13}$$

In some research the error ϵ_{r21} ignore the error and thus TEC can be obtained using equation 2.14 [Poh and Kamarudin, 2006].

$$TEC = \frac{R2–R1}{\frac{40.3}{f_2^2} - \frac{40.3}{f_1^2}} = 9.5196x10^{16}(R2 - R1) \tag{2.14}$$

Here, R1 and R2 are the pseudo-range measurements from L1 and L2 respectively.

The ionosphere fluctuates more near the equator and the magnetic poles and it is more calm around the mid-latitudes [Misra and Enge, 2001]. Uganda is situated at the equator and the highest ionospheric delay and disturbances occur between 0° and 20° North and South of the magnetic equator. Solar flares can cause large and rapid fluctuation in electron density, which can cause for problems in tracking the GPS signal. For these reasons Uganda is chosen as study area. When looking at figure 2.4 and 2.5, it is clearly visible that the total electron content, which is related to the ionospheric delay, is higher at the equator and it fluctuates more at the equator during the seasons and a solar cycle.

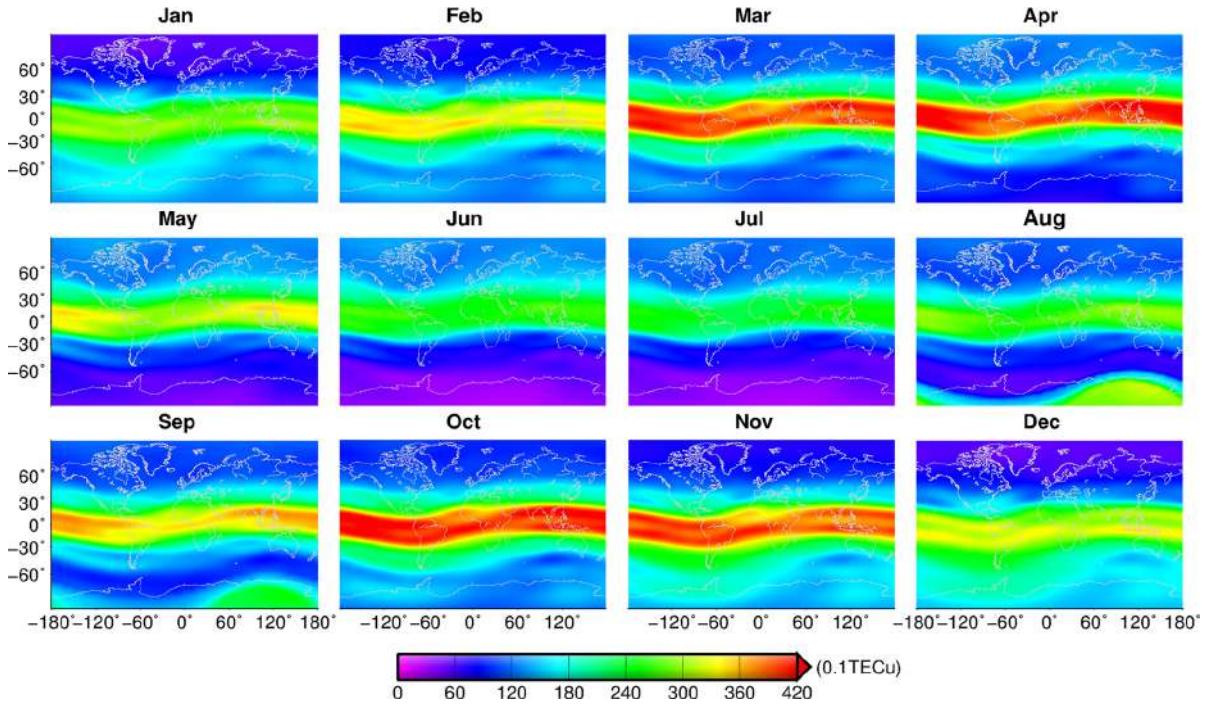

Figure 2.4: Spatial distribution of the seasonal total electron content [Guo et al., 2015]

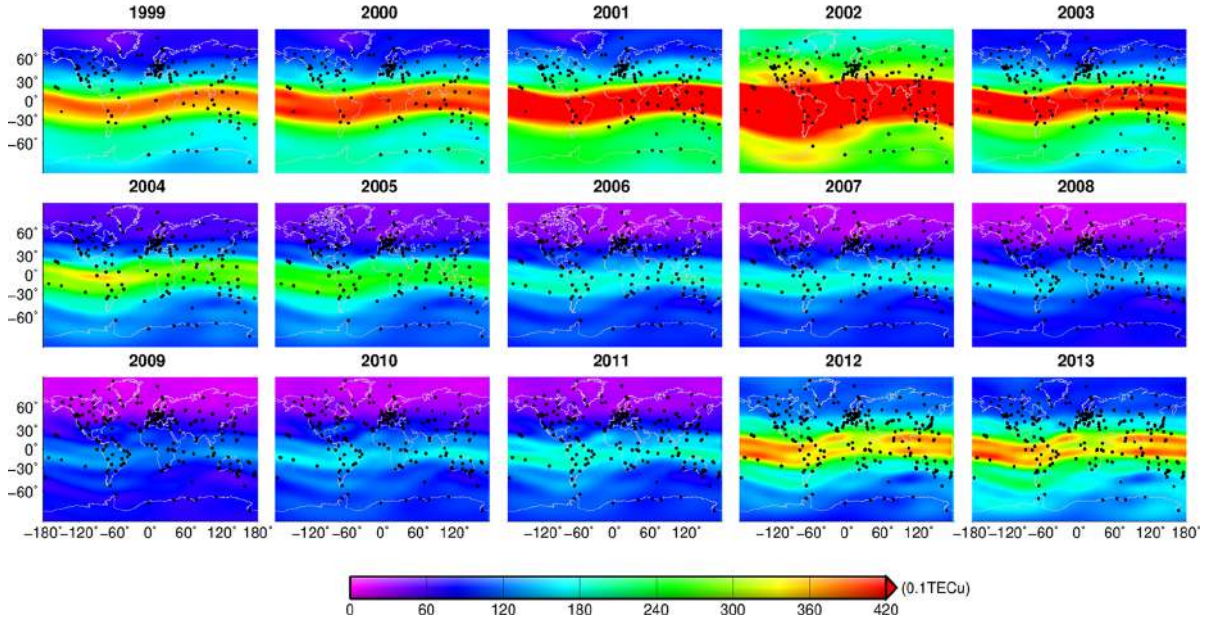

Figure 2.5: Spatial distribution of the annual total electron content for one solar cycle [Guo et al., 2015]

For dual-frequency measurements the ionospheric delay can be eliminated using the ionosphere-free combination. The ionospheric delay estimation for dual-frequency measurements using the code measurements can be found in equation 2.15 for L_1 and in equation 2.16 for L_2 [Misra and Enge, 2001].

$$I_{L1} = \frac{f_{L2}^2}{f_{L1}^2 - f_{L2}^2}(\rho_{L2} - \rho_{L2}) \tag{2.15}$$

$$I_{L2} = \frac{f_{L1}^2}{f_{L1}^2 - f_{L2}^2}(\rho_{L2} - \rho_{L2}) \tag{2.16}$$

The ionospheric delay for the carrier phase measurement can be found in equation 2.17 for L_1 and in equation 2.18 for L_2 [Misra and Enge, 2001].

$$I_{L1} = \frac{f_{L2}^2}{f_{L1}^2 - f_{L2}^2}[\lambda_{L1}(\rho_{L1} - N_{L1}) - \lambda_{L2}(\rho_{L2} - N_{L2}] \tag{2.17}$$

$$I_{L2} = \frac{f_{L1}^2}{f_{L1}^2 - f_{L2}^2}[\lambda_{L1}(\rho_{L1} - N_{L1}) - \lambda_{L2}(\rho_{L2} - N_{L2}] \tag{2.18}$$

For single-frequency measurements the SEID model will be used in research, which will be explained in section 3.2.

2.2.3.2. Tropospheric delay

The troposphere is an atmospheric layer, which starts at the Earth's surface and can reach up to 20 km above sea level [Teunissen and Montenbruck, 2017]. Moreover, also the troposphere causes the GPS signal to refract. The troposphere is dispersive for GPS frequencies [Misra and Enge, 2001]. This means that the refraction does not depend upon the frequency of the signal. Since 99% of all water vapor and aerosols in atmosphere can be found in the troposphere, it has an important effect on the speed of propagation of GPS signal [Teunissen and Montenbruck, 2017]. The tropospheric delay can be divided in two components:

- 1. The tropospheric wet delay
- 2. The tropospheric dry delay

The dry and wet delay affect the propagation of the GPS signal differently. The spatial and temporal distribution of the water vapor, and thus the wet delay, is highly variable [Teunissen and Montenbruck, 2017]. This high variability makes the tropospheric wet delay difficult to compute. The spatial and temporal variation of the dry delay is much less [Teunissen and Montenbruck, 2017]. However, compared to the ionospheric delay the tropospheric delay has a lower variability [Misra and Enge, 2001]. The tropospheric delay significantly changes only in the wet component [Misra and Enge, 2001]. The tropospheric delay can be written as

$$\tilde{T} = 10^{-6}\int N(l)dl = 10^{-6}\int [N_d(l) + N_w(l)]dl = \tilde{T_d} + \tilde{T_w} \tag{2.19}$$

In equation 2.19 dry and wet delay are respectively $\tilde{T_d}$ and $\tilde{T_w}$ and the integration is along the signal path. How to compute the refraction of the dry gases and the water vapor in the troposphere is formulated in equation 2.20 and 2.21.

$$N_d = 77.64\frac{P}{T} \tag{2.20}$$

$$N_w = 3.73 * 10^5\frac{e}{T^2} \tag{2.21}$$

Here, P is the total pressure and e is the partial pressure of the water vapor [Misra and Enge, 2001]. T is the temperature in Kelvin [Misra and Enge, 2001]. The tropospheric delay can be determined by using precise point positioning services as NRCan. More information about NRcan can be found in section 3.3.

3

Determining ionospheric delay

3.1. Equipment

3.1.1. Dual frequency receivers

The dual frequency receivers are used as reference stations. For computing the ionospheric delay by using the SEID model with single frequency receivers in a small scale network at least three dual frequencies are recommended as reference stations. By using multiple reference stations problems like missing data will be avoided as well as it improves the reliability of the data [Deng et al., 2011]. The dual frequency receivers used for this research are the GPS dual frequency stations: Trimble 5700 receiver with a Zephyr Geodetic Trimble antenna. These dual frequencies receivers were provided by the faculty of Civil Engineering & Geosciences of the Delft Technical University of Technology.

3.1.2. Single frequency receivers

As a single frequency receivers u-blox NEO-M8T are used. For this research two different antennas are bought to look if the multipath error has a huge effect on the results. Three patched antenna's are used, which are high performance active GPS patched antenna. The other antenna's are Tallysman TW3470 antenna's, which are more suitable to handle multipath signal.

3.2. SEID model

Since water vapor and the zenith total delay have a high spatial variability, interpolation of these parameters derived by dual frequency GPS receivers do not have a sufficient quality for weather prediction applications [Deng et al., 2012]. Deng et al. (2012) states that the ionospheric delay can be interpolated in a plane. However, the ambiguity parameter for the carrier observations in the ionospheric delay observation is a major obstacle in the spatial reconstruction of the ionospheric delay. The ionospheric delay from the reference stations cannot be interpolated directly to the single frequency receiver stations inside the area of the dual frequency receiver. For these reasons the SEID model is used in this study to compute the ionospheric delay at the location of the single frequency receivers. .

To solve the ionospheric delay for the single frequency receivers the Satellite-specific Epoch-differenced Ionospheric Delay model (SEID) is used in this research. The model is explained in the article "Retrieving tropospheric delays from GPS networks densified with singe frequency" receivers by Deng et al (2009). It is important to know that the SEID model can be used only to compute the ionospheric delay under normal ionospheric conditions [Deng et al., 2009].

Furthermore, there are some requirements for using the SEID model. These are:

- At least 3 reference dual frequency receivers are needed to run the SEID model.
- Densification of a existing network with SF receivers.
- Baseline should be longer than 10 km.

For the SEID model an epoch-differenced delay will be applied. Before using the model phase center corrections need to be applied in advance [Deng et al., 2009].

In this research the phase center corrections are not applied so the same non-dispersive delay ($\xi(j)$) is used for different frequencies [Deng et al., 2009]. The non-dispersive delay represents the geometric delay, tropospheric delay and the clock biases.

First the epoch-differenced delay is computed for the SEID model. Here, the first observation of the satellite supposes to be at epoch j_0 and it is constantly tracked until epoch $j_0 + k$ [Deng et al., 2009]. In Deng et al. (2009) the difference in ionospheric delay between the epochs j_0 and $j_0 + k$ at the carrier phase frequency (L_1) is described as:

$$\delta D_1(j_0, j_0 + k) = D_1(j_0 + k) - D_1(j_0) \tag{3.1}$$

For this research as in Deng et al (2009) the epoch-differenced delay will be computed for all epochs of the carrier-phase (L) as:

$$L_i(j_0 + k) + \gamma_i \delta D_1(j_0, j_0 + k) = \xi(j_0 + k) - D_i(j_0) + \lambda_i N_i \tag{3.2}$$

In Deng et al (2009) γ_i is computed as follow:

$$\gamma_i = f_i^2 / f_1^2 \tag{3.3}$$

In equation 3.2 ξ represents the non-dispersive delay, λ represents the wavelength and N is the ambiguity. The frequency is displayed as f in equation 3.3.

In equation 3.2 $D_i(j_0)$ and N_i can be merged as $\lambda_i \overline{N}_i$ to create an observation equation equivalent to the ionospheric-free observations [Deng et al., 2009].

$$L_i(j_0 + k) + \gamma_i \delta D_1(j_0, j_0 + k) = \xi(j_0 + k) + \lambda_i \overline{N}_i \tag{3.4}$$

To process the single frequency data the epoch-differenced ionospheric delay δD from equation 3.4 is being used [Deng et al., 2009].

The difference of the ionospheric observations is L_4 used for a ionospheric delay model is formulated as:

$$L_4 = L_1 - L_2 = \lambda_1 N_1 - \lambda_2 N_2 - (D_1 - D_2) \tag{3.5}$$

For the SEID model an epoch-differenced ionospheric delay is sufficient to use to compute the second frequency. Therefore, for the SEID model the equation 3.5 changes in equation 3.6.

$$\delta L_4(j, j+1) = \delta D_1(j, j_1) - \delta D_2(j, j+1) = \frac{f_1^2 - f_2^2}{f_1^2} \delta D_1(j, j_1) \tag{3.6}$$

The ionospheric delay is determined using the three dual frequency receivers. After that the epoch differenced ionospheric delay is computed at these dual frequency station. After that the epoch differenced delay is interpolated to the location of the single frequency using inverse distance interpolation, where p=2. A correction will be calculated for all single frequency receivers inside the network as $\delta \tilde{L}_4(j, j+1)$ [Deng et al., 2009].

The correction for epoch k is the sum of the epoch-differenced correction and it is formulated in Deng et al (2009) as:

$$\tilde{L}_4(j_0, k) = \sum_{j_0}^{k-1} \delta \tilde{L}_4(j, j+1) \tag{3.7}$$

In order to process the single frequency receiver in the same way, a second carrier phase observation L_2 is generated by adding the $\tilde{L}_4(j_0, k)$ to the carrier phase observation L_1 [Deng et al., 2009].

$$\tilde{L}_2(k) = L_1(k) + \tilde{L}_4(j_0, k) \tag{3.8}$$

The second carrier phase observation $\tilde{L}_2(k)$ is similar to the first carrier phase observation L_1. The difference between $\tilde{L}_2(k)$ and L_1 is that $\tilde{L}_2(k)$ is corrected for the ionospheric delay of the second frequency [Deng et al., 2009].

Deng et al. (2009) states that the pseudo-range observation is not as important as the carrier-phase measurements. Therefore, no epoch-differenced method is used.

The SEID model computes the second psuedo-range measurement directly, which is formulated in Deng et al. (2009) as:

$$C_4 = C_1 - C_2 = D_{C1}(k) - D_{C2}(k) \tag{3.9}$$

$$C_2(k) = C_1(k) - D_{C1}(k) + D_{C2}(k) \tag{3.10}$$

An overview of all processing steps explained in this section 3.2 are visualized in a flowchart in figure 3.1.

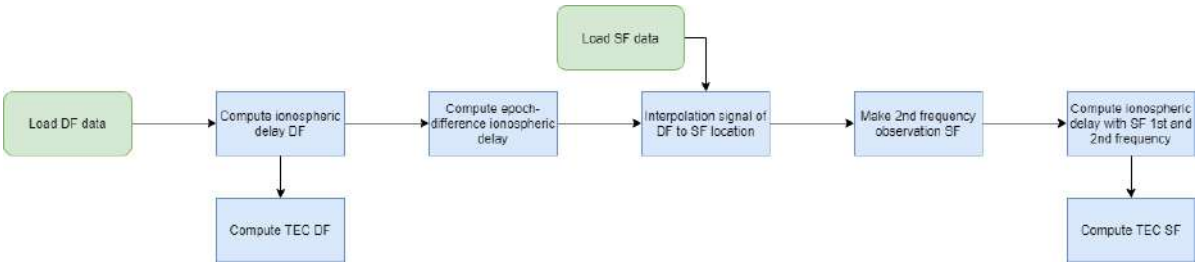

Figure 3.1: Flowchart of the processing steps in this research

3.3. Further processing of data: Precise point positioning (PPP)

When using the single frequency data, after creating the second frequency (L2) for the single frequency receiver, the data is needed to processed using the precise point positioning technique (PPP).

Precise Point positioning (PPP) is a technique which uses undifferenced, dual-frequency, pseudo-range and carrier observations and GNSS satellite clock and orbit corrections, generated from a network of global reference stations, to provide a high level of accuracy for static or kinematic point positioning [Zumberge et al., 1997, Teunissen and Montenbruck, 2017]. In addition to a high accuracy of point positioning, the PPP provides tropospheric zenith path delay (ZTD), which is important for weather forecasting [Zumberge et al., 1997, Teunissen and Montenbruck, 2017, Krietemeyer et al., 2018]. Using the PPP approach the receiver position, receiver clock offset and tropospheric zenith delay are computed [Teunissen and Montenbruck, 2017]. For the carrier-phase observations, the PPP also estimates the initial phase ambiguities for all satellites [Teunissen and Montenbruck, 2017]. The PPP approach can be used for a single receiver. However, it is important to keep in mind that this approach uses a network of global reference stations to compute the satellite orbits and clocks, which are needed for the implementation [Teunissen and Montenbruck, 2017]. One of the web processing tool for precise point positioning (PPP) is called NRCAN. At the moment of the research, version 2.18.0 was available. CSRS-PPP tool of NRCAN allows the computation of higher accuracy positions of raw GNSS data [Natural Resources Canada, 2019]. The satellite ephemerides information, transmitted by the satellites, is used to compute a corrected position with an constant high absolute accuracy of the receiver [Natural Resources Canada, 2019]. This is done by uploading the RINEX data from the dual-frequency receiver or the new created dual-frequency rinex from the single frequency on the website. The website process data in static (fixed receiver) and kinematic mode (moving receiver) [Natural Resources Canada, 2019]. Once the corrections are computed, they are delivered to the end user over the internet. These corrections are used by the receiver, resulting a high accuracy positioning with no base station required [Teunissen and Montenbruck, 2017].

4

Network set-up

The research took place around the capital city of Uganda, Kampala. In this chapter, the ideal network set-up, the experimental set-up for both measuring rounds and the problems faced in this research, will be discussed. During the research two measurements rounds were executed. One network was set up at the western part of Kampala and the other one was set up more to the east.

For all networks set-ups the dual frequency receivers (TRIMBLE 5700) were distributed whereas the single frequency receivers (ublox NEO-M8T) were placed between or around the dual frequency receivers. The TRIMBLE 5700 receivers were connected to the electricity network, whereas the ublox receivers had a power supply from powerbanks that lasted about 58 hours.

4.1. Ideal network

Multiple researchers densified their GPS network with single and dual frequency receivers to improve the weather forecast [Deng et al., 2009, Bender et al., 2011, Krietemeyer et al., 2018]. To compute the ionospheric delay with a high accuracy the GPS network of dual frequency receivers should be densified with single frequency receivers having an inter-station distance below 20 km [Bender et al., 2011, Rocken et al., 2000]. The goal of this densification of the network was to provide information on the spatial variability of atmospheric delay and in this case it was the ionospheric delay [Braun et al., 1999]. This densification with single frequency receivers can lead to better estimation of the ionospheric delay if the SF receivers are placed between the existing DF receivers [Deng et al., 2011]. A decreasing distance between single and dual frequency station can lead to an increasing accuracy in the estimated ionospheric delay [Deng et al., 2011]. This is because the densified network can compute small-scale ionospheric fluctuation [Rocken et al., 2000]. Normally, sparse networks (>150 km) only capture large-scale features of the ionosphere and thus does not allow to get ionospheric delay with mm accuracy [Rocken et al., 2000]. Moreover, the ionospheric error will also be minimized by keeping the distance between the station below 20 km, since the variation of the ionosphere is small on short distances [Braun et al., 1999].

4.2. Network set-up Uganda

For the network set-up secured locations were chosen to install the equipment. Furthermore, these locations should ideally have a clear view to the sky and the devices should be installed at undisturbed locations such as roofs or on top of watertanks. In the researches of Stierman (2017) and Koning (2017), locations like schools and embassy building were chosen. During the fieldwork campaign it was difficult to find locations, which allowed to set up a single or dual frequency receiver. Therefore, some of the locations of Koning (2017) and Stierman (2017) were again used as measurement locations, since these locations allowed and could provide a secure spot to set up the equipment.

4.2.1. Network set-up round 1

In the first measurement round the dual frequency receivers were placed in different towns to get a good baseline between the different stations.

On the 18th of September 2018, a dual-frequency receiver was set up on the roof of the Department of Zoology, Entomology and Fisheries Sciences at the Makerere University in Kampala. The roof was quite flat and it had a clear view to the sky. At the time of installing the equipment it was a bit windy.

On the 19th of September, the other two dual frequency receivers were set up at the Ndejje Secondary School and in Buloba at the neighbor's house of Richard Cliffe. At the Ndejje Secondary School the dual frequency receiver was set up on a flat roof where also a watertank is located. The watertank can have an increasing multipath effect. In Bulado the dual frequency was set on a flat roof but there was an television antenna located next to the receiver. Both locations had a clear view to the sky.

Figure 4.1: Measurement set-up for a dual frequency reicever at Ndejje Secondary School

The single frequency receivers were placed around and in between the dual frequency receivers. All single frequency receivers were set-up on the same day, namely on the 19th of September 2018. There were in total five single frequency receivers with two different antennas. Two tallysman antennas were used and three patched antennas were used in this measurement round. One tallysman single frequency receiver was positioned on the watertank at Makerere High School in Migadde. Another tallysman antenna was positioned on the watertank at Richard Cliffe's house. This distance between the single frequency receiver on the watertank at Richard's house and the dual frequency receiver on the roof of Richard's neighbours house was approximately 15 meters. The single frequency receivers with the patched antenna's were placed Bulabo High School, Onwards & Upwards High School in Buloba and at Mutty House in Kampala.

Figure 4.2: Setting up a single frequency receiver at Richard Cliffe house

At Onwards & Upwards High School the single frequency receiver was set up on the roof of the administration building, which had a corrugated iron roof. Only a small part of the view to the sky was blocked by a higher corrugated iron roof. At Buloba High school the single frequency receiver with the patched antenna was positioned on a brick on the roof of a building which was under construction. The roof had a flat surface with a clear sky. Due to rainfall that day the roof had been partly flooded, so a brick was used to set up the device on a dry surface. At Mutty House in Kampala the single frequency antenna with patched antenna was positioned on an unstable surface, but which had the best view to the sky. However, it is important to keep in mind that at this location the view to the sky was partially blocked by a fench.

For this research the measurements were used, which were obtained on the 20th of September. After obtaining the measurements, the dual frequency receivers were checked if the GPS antenna was still levelled after taking the measurements. For the first measurement round the antennas of the dual frequency receiver were still leveled for all three locations.

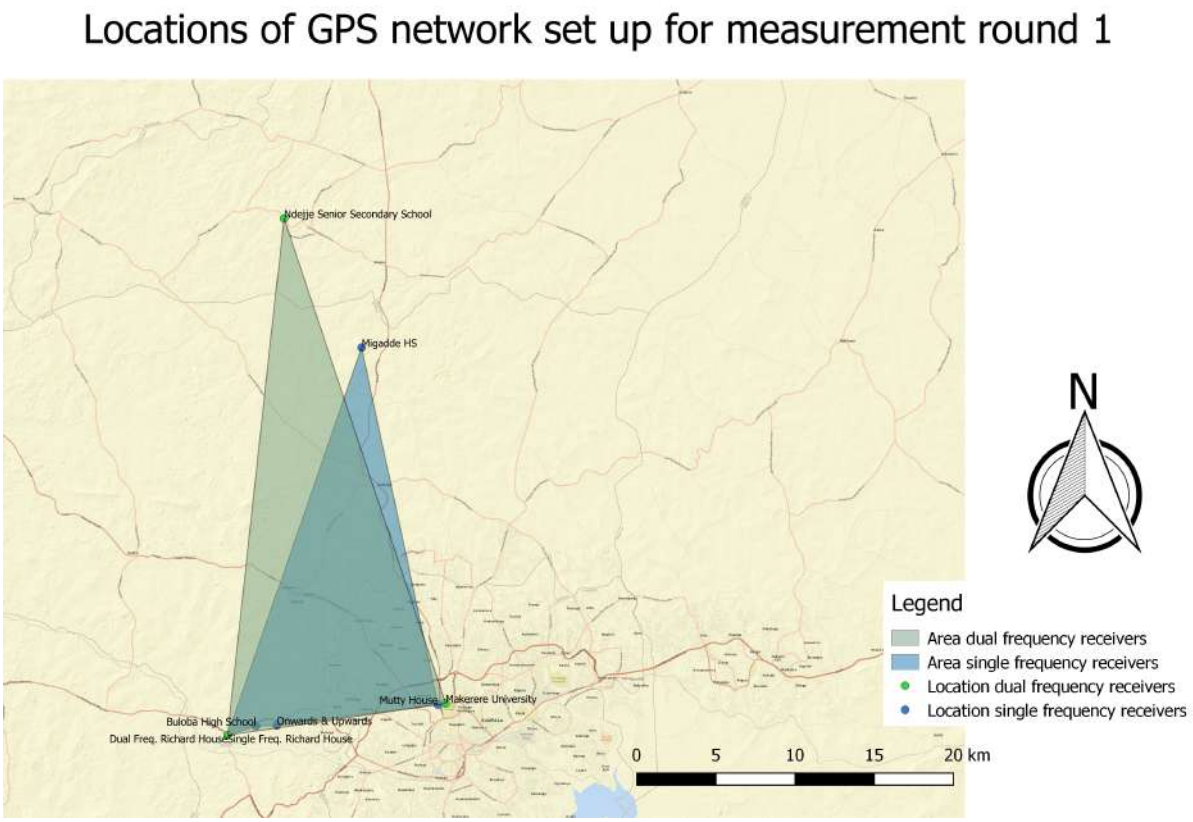

Figure 4.3: Overview of the measurement network set up for measurement round 1

4.2.2. Network set-up round 2

For the second measurement round, difficulties occurred in getting permission to set up the GPS receivers on secure locations. Therefore, for the second measurement round two dual frequency receivers stayed at the same location as in the first round. These were the dual frequency receiver positioned in Kampala and Ndejje. On the 12th of October the third dual frequency receiver was positioned at Wanyange Girls Secondary School. The dual frequency receiver was positioned on the guard house. On the 29th October the dual receiver were collected at Wanyange Girls Secondary School. When collecting the dual frequency receiver the equipment was checked. At the moment of collecting the device the antenna was still level.

On the 23th of October the single frequency receivers were dispatched for the second measurements round. The second measurement day was on 24 October 2018. The single frequency receivers with the Tallyman antenna were set up at the World Ahead Secondary School in Matugga and at the Uganda Christian University (UCU) in Mukono. The single frequency receivers with the patched antenna were set-up at Gayaza High School in Gayaza, at the house of Yvonne de Haan in Kampala and at the TAHMO office in Kampala.

The single frequency receiver at UCU was positioned on a plateau at the first floor, which had a clear view of the sky. Close to the plateau there was a roof. When the single receiver was picked up, it looked like that the equipment setting was undisturbed. At the house of Yvonne de Haan the single frequency receiver was positioned on the guard house, which had clear view of the sky. The roof consisted of corrugated iron roof. The receiver was picked up on the 26th of October. It had a partial clear view to sky, because of the trees close to the guard house. At World Ahead Senior Secondary School in Matugga the single frequency receiver was tapped on the iron structure of the watertank tower, which had a clear view of the sky. An overview of how the measurement location looked like can be seen in figure 4.4.

Figure 4.4: Measurement set-up at World Ahead Secondary School. The Tallysman antenna is taped to the iron structure of the watertank tower.

A single receiver was positioned at the Gayaza high School, where the receiver had been set up on the roof of the building of the secretariat. The roof consisted of corrugated iron and it had a clear view to the sky.

At the TAHMO office the single frequency receiver was positioned at the roof of a fourth floor building. It was positioned on top of a watertank, which had a clear view of the sky, see figure 4.5.

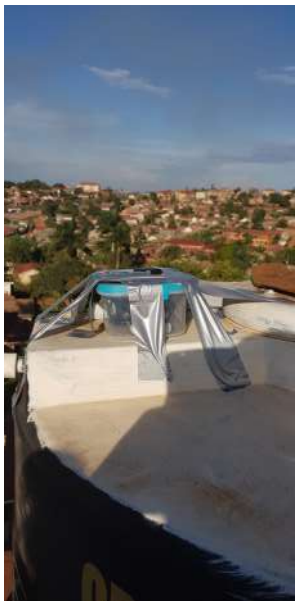

Figure 4.5: Measurement set-up at TAHMO office

After retrieving the dual frequency receiver at Ndejje High School, it was discovered that equipment was turned off. Looking at the data the receiver had stopped logging three days after retrieving the data from measurement round one. While talking with the employees of that school, power breaks occurred in the time between our previous visit, which can be the cause of our equipment failure. At other locations no equipment failure occurred.

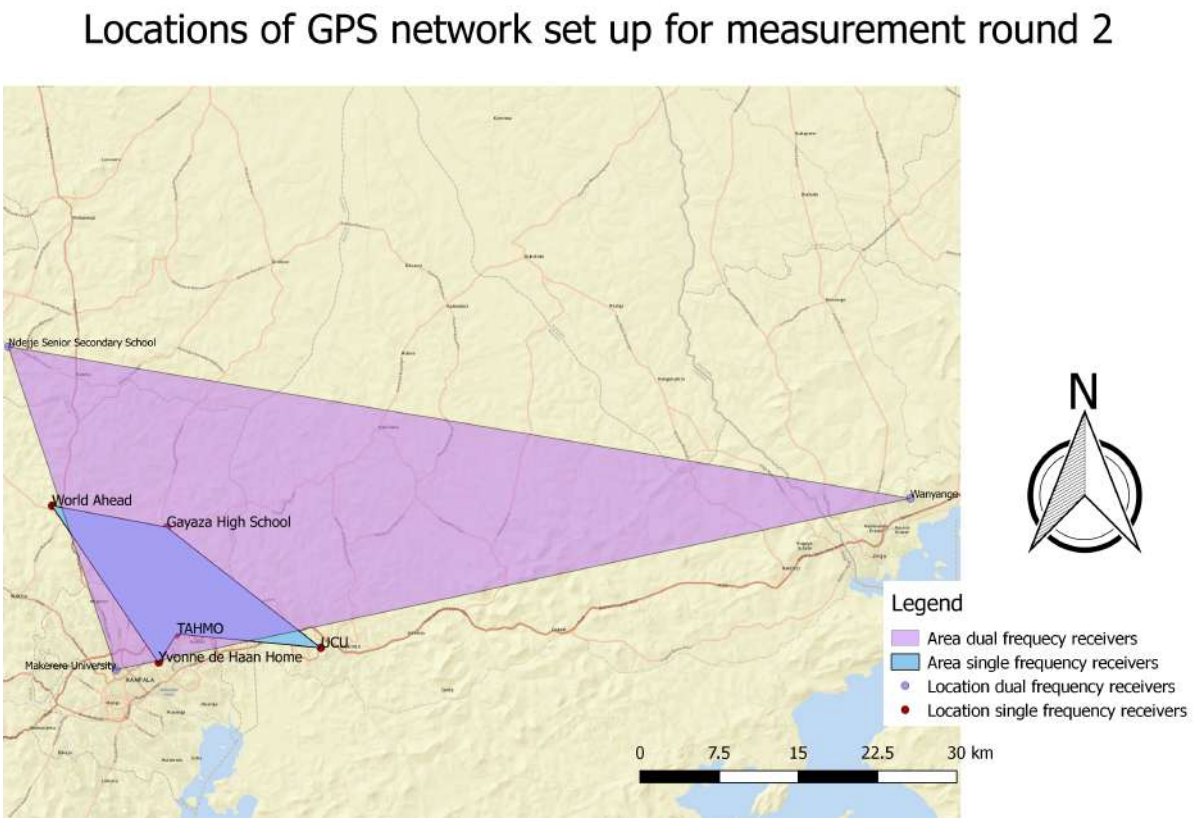

Figure 4.6: Overview of the measurement network set up for measurement round 2

5

Results & discussion

Data of the first measurement round are discussed only in this chapter, because in the second measurement round the dual frequency receiver at Ndejje Secondary School has stopped logging.

5.1. Ionospheric delay of the dual frequency receivers

Using the ionospheric-free combination for dual frequency receivers explained in section 2.2.3.1 the ionospheric delay for the code-code and carrier-carrier are computed. Here, the code-code ionospheric delay measurements are computed using only the code measurements. The carrier-carrier ionospheric delay measurements are computed using only the carrier phase measurements measurements. The figures below are showing the results.

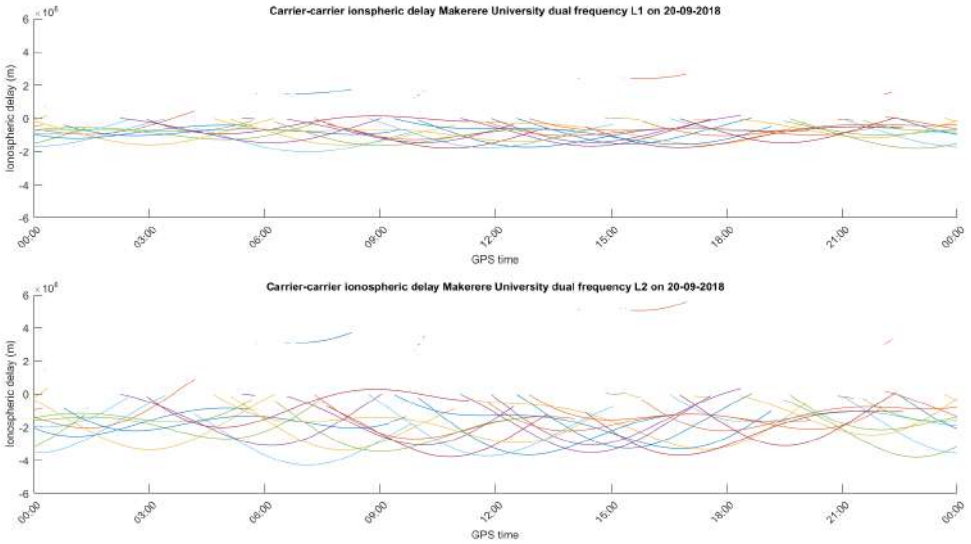

Figure 5.1: Carrier-carrier ionospheric delay measurement for the dual frequency receiver at Makerere University, Kampala. The different colors represent the processed signals received from the different GPS satellites. The figure shows the ionospheric delay for one entire day.

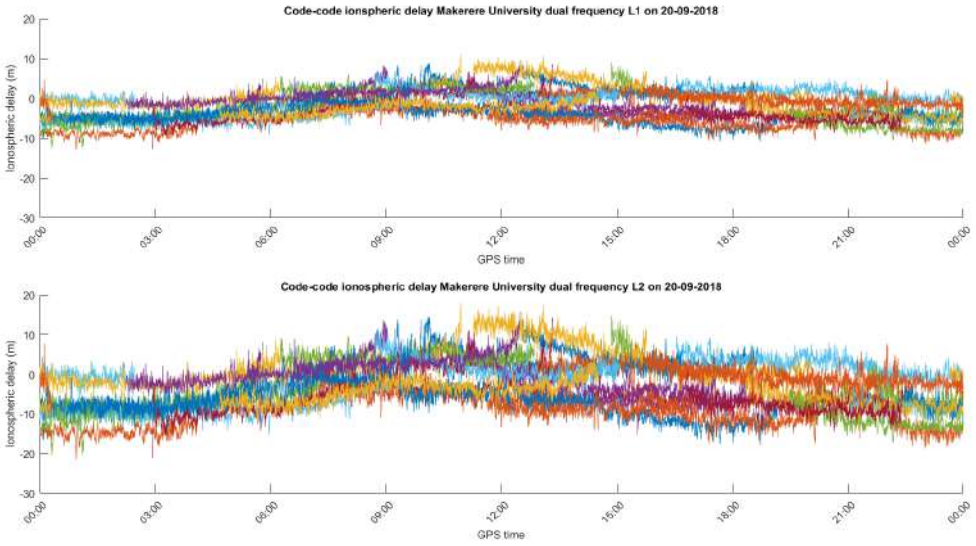

Figure 5.2: Code-code ionospheric delay measurement for the dual frequency receiver at Makerere University, Kampala. The different colors represent the processed signals received from the different GPS satellites. The figure shows the ionospheric delay for one entire day.

In figure 5.1 and figure 5.2 the ionospheric delay at Makerere University is plotted. The different colors in the figures visualize the signal of the different GPS satellites. There is a clear difference in showing the variation in ionospheric delay when the code-code and phase-phase plots are compared. The carrier-carrier plots have a much larger variation in ionospheric delay than the code-code plots. Usually, the phase measurements have a higher precision in the ionospheric delay than the code measurements. For getting a high precision phase measurements ambiguities must be resolved. However, in this case the ambiguities are not resolved. The carrier phase data is biased by ambiguities. Misra and Enge (2001) describe that carrier phase measurements are accurate in the absence of huge multipath errors. As can be seen in figure 5.1 discontinuities in the signal are visible, which are called cycle slips. These cycle slips are caused by phase breaks in the signal. The cycle slips introduce an offset in the observation time series at around 7:30, 16:30 and 22:30. These cycle slips cause a change in ambiguity, hence the offset. The cycle slip in figure 5.1 can be caused by a power loss, a very low signal-to-noise ratio, a failure of the receiver or severe ionospheric conditions [Van Sickle, 2017]. After each cycle slip the carrier phase ambiguities change and therefore bias at that point will be different.

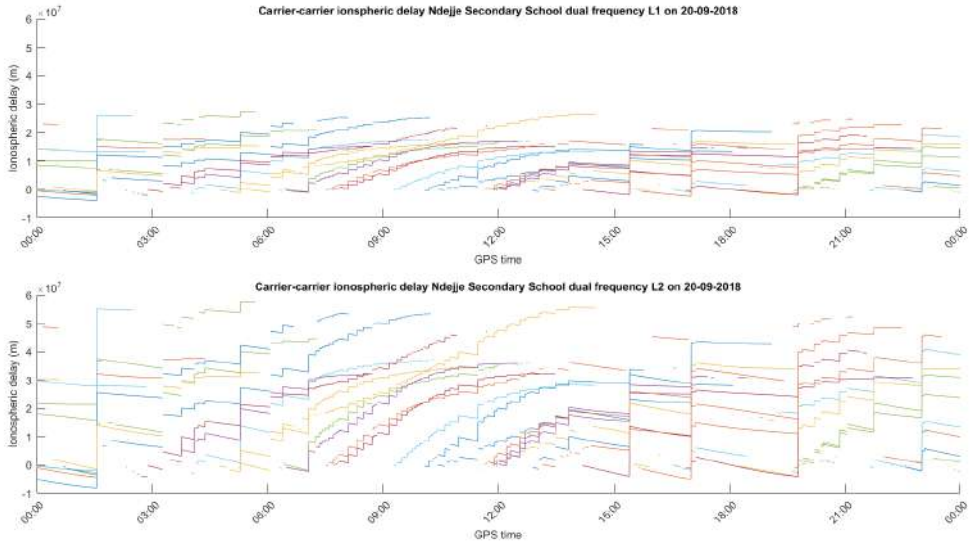

Figure 5.3: Code-code ionospheric delay measurement for the dual frequency receiver at Ndejje Secondary School. The different colors represent the processed signals received from the different GPS satellites. The figure shows the ionospheric delay for one entire day.

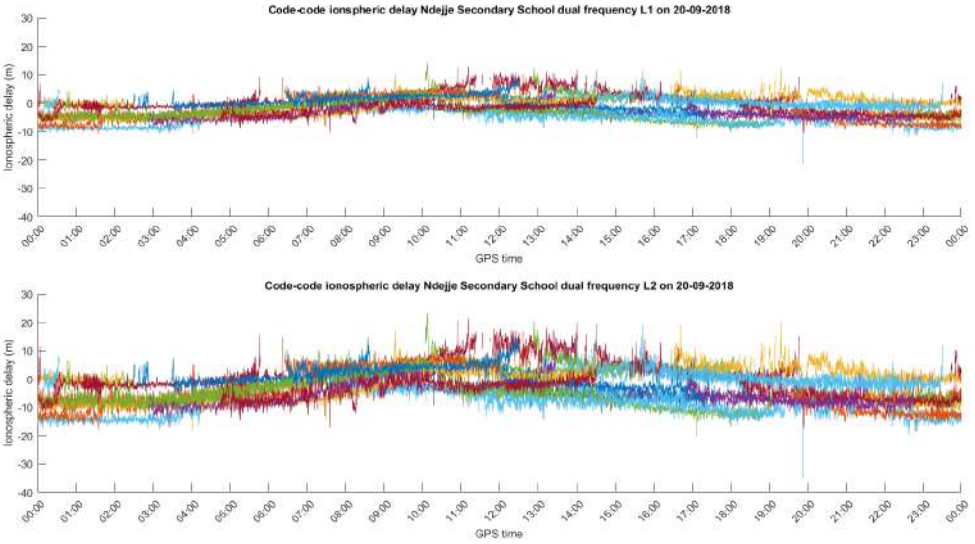

Figure 5.4: Code-code ionospheric delay measurement for the dual frequency receiver at Ndejje Secondary School. The different colors represent the processed signals received from the different GPS satellites. The figure shows the ionospheric delay for one entire day.

Figures 5.3 and 5.4 show the ionospheric delay of code and carrier phase measurements. When looking at the carrier phase measurements in figure 5.4 a lot of jumps occur in the data. When looking only at the measured epoch of the observations, these jumps occur every 11th epoch. Usually the difference between epoch t and epoch t+1 have the same δt (time difference). However, when computing δt every 11th epoch has a different δt compared to the other 10th epochs. At every 11th epoch a clock reset occur and these are called clock jumps. At every clock jump the carrier phase ambiguity changes. Looking at the carrier phase measurements of the Ndejje Secondary School a receiver measurement error takes place. Furthermore, the dual frequency receiver at the Ndejje Secondary School receives at certain epochs only 2 GPS signal whereas the receivers needs to have receive at least 4 GPS signals to resolve the ambiguities and biases, for example the receiver clock bias.

The ionospheric delay of the third dual frequency station can be found in appendix B.

5.2. Epoch-difference ionospheric delay

In this section the epoch-difference ionospheric delay is discussed for Buloba dual frequency station, because the epoch-difference ionospheric delay of this receiver has the biggest weight in the inverse distance interpolation in the SEID model. As part of the SEID model the epoch-difference ionospheric delay of the dual frequency receivers are computed. Looking at the epoch difference ionospheric delay of the Buloba dual frequency station a few outliers are visible at 14:00 and around 20:30 and 20:45. Although some outliers occur throughout the entire day, the epoch-difference ionospheric delay changes per epoch in centimeters accuracy. Lastly, the fluctuation in the signal is clearly visible. The fluctuation in the signal is the noise of the signal.

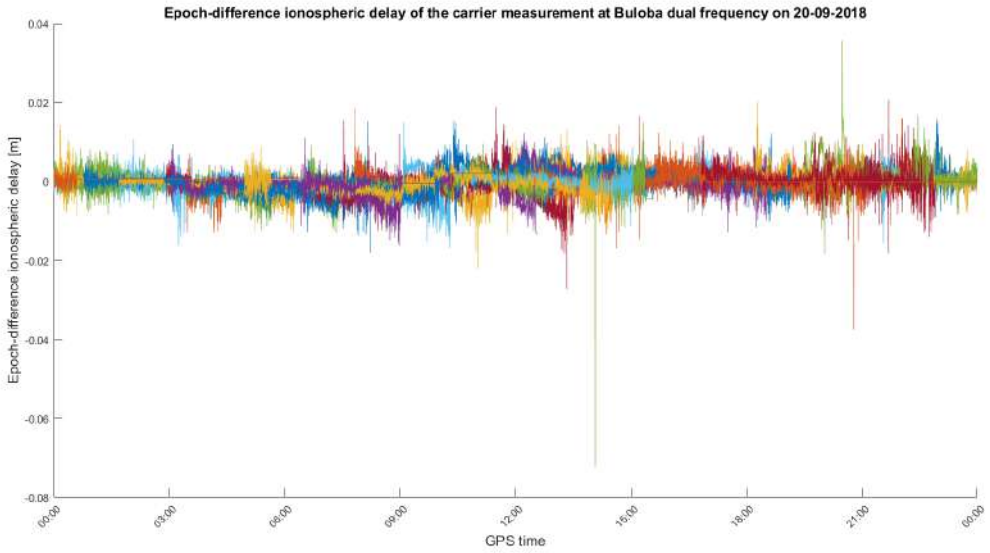

Figure 5.5: Epoch-difference ionospheric delay at Richard's neighbour house, Buloba. The different colors represent the processed signals received from different the GPS satellites. The figure shows the epoch-difference ionospheric delay for one entire day.

While looking at figure 5.6 the epoch-difference ionospheric delay of the carrier measurement at Ndejje Secondary School consists of more outliers than the results of the dual frequency receiver in Buloba. Moreover, the outliers of the epoch-difference ionospheric delay are larger, namely 10^6, which is a megameter. Thus, the epoch-difference ionospheric delay in the outliers are longer than the height of the ionospheric layer. A reason for these outliers can be the cycle slipes and the clock error occurring every 11th epoch.

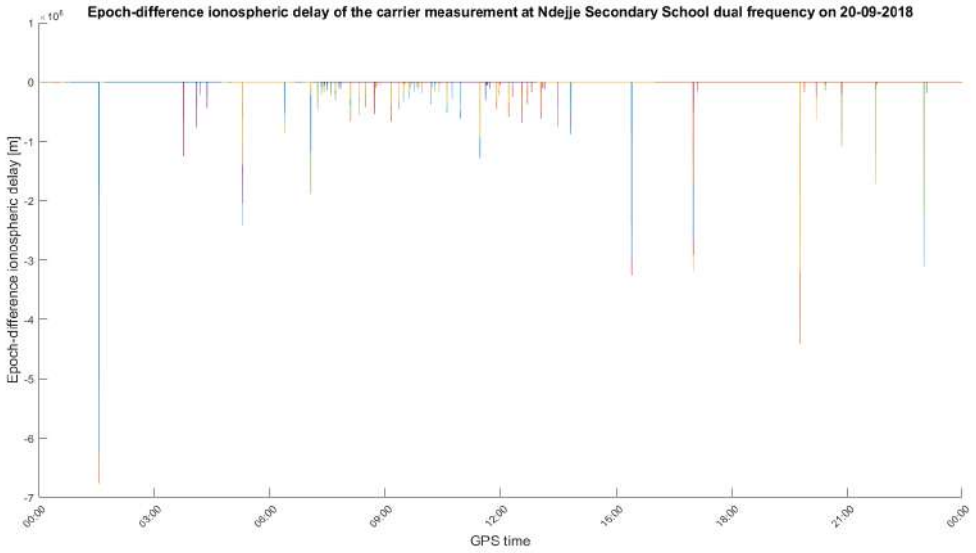

Figure 5.6: Epoch-difference ionospheric delay at Ndejje Secondary School. The different colors represent the processed signals received from the different GPS satellites. The figure shows the epoch-difference ionospheric delay for one entire day.

The epoch-difference ionospheric delay of the dual frequency receiver at Makerere University can be found in appendix C.

5.3. Ionospheric delay of the single frequency receivers

The ionospheric delay for two single frequency receivers are visualized in this section, which are the single frequency receiver at Onwards & Upwards High School and the single frequency receiver at Richards House, both in the town called Buloba. The receiver at Onwards & Upwards has a patched antenna and the receiver at Richard House has a Tallysman antenna, which should decrease the multipath error. Both these receivers are chosen since they are located the farthest away from the dual frequency receiver in Ndejje. Since the single frequency receivers have a time sampling rate of 1 second and the dual frequency receivers have a time sampling rate of 15 seconds, the single frequency data is downsampled with a time sample interval of 15 second. This time sample interval is used for computing the second frequency of the single frequency receiver. Furthermore, the single frequency receiver looked at all GNSS stations. For this research only the GPS constellation is used, which consists of 32 GPS satellites. The data is processed using the SEID model, which is described in section 3.2. Looking at the ionospheric delay computed at the single frequency receiver, it is clear that there are more ambiguity resets than at the dual frequency receiver. When computing the second frequency only satellites at a certain epoch, which are visible at the single frequency receiver as well as a dual frequency receiver is used. Looking at figure 5.7 the clock jumps in the dual frequency receiver of Ndejje Secondary School have a huge influence on the carrier signal. Since every 11th epoch a clock jump is occurring, at every 11th epoch the ambiguity resets. When no resets occur, it can be assumed that these satellites are not visible at Ndejje Secondary School, but the signal of these satellites are logged by one or both dual frequency receiver. Because of the clock jump at every 11th epoch by the dual frequency receiver of Ndejje Secondary School no accuracy study has been done on the computed ionospheric delay of figures 5.7 and 5.8.

Since the code measurements are unambiguous the clocks jumps do not have a huge influence on the signal. For both receivers the ionospheric-free combination is used to compute the ionospheric delay.

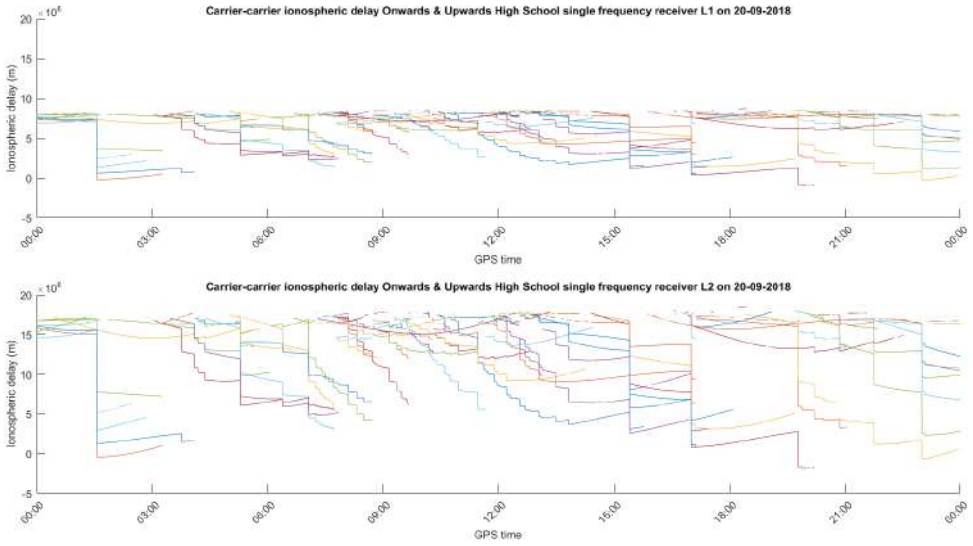

Figure 5.7: Carrier-carrier ionospheric delay at the single frequency receiver Onwards & Upwards High School. The different colors represent the processed signals received from the different GPS satellites. The figure shows the ionospheric delay for one entire day.

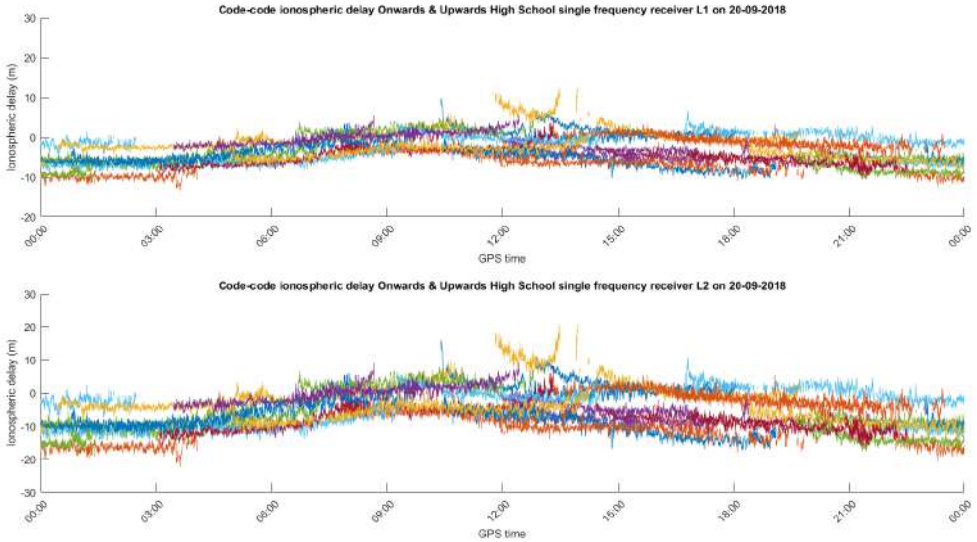

Figure 5.8: Code-code ionospheric delay at the single frequency receiver Onwards & Upwards High School. The different colors represent the processed signals received from the different GPS satellites. The figure shows the ionospheric delay for one entire day.

Like in Deng et al. (2011) most of single receivers are located at the outer boundaries of the dual frequency area, where these locations are visualized in figures 4.3 and 4.6. Like in the article of Deng et al. (2011) it can be assumed that the accuracy of the ionosphere correction with the SEID method is affected by the unbalanced distribution of the dual frequency receivers around the single frequency receivers [Deng et al., 2011]. Some receivers are installed near the network boundaries or at other unfavorable positions with no clear view of the sky. One of these single frequency receiver close to the network boundaries is the single frequency at Richard's house. Figures 5.9 and 5.10 show the ionospheric delay at Richard's house. For Richard's house only the closest dual frequency receiver is used to interpolate the signal to the SF location. This dual frequency is located with a distance of approximately 15 meters away from the single frequency receiver at Richard's house. This approach is chosen, because it is expected that ionospheric delay does not change spatially in such a short distance. Secondly, by using this approach the computed ionospheric is not affected by the failed dual frequency receiver at Ndejje Secondary School.

However, Deng et al. (2009) states that a requirement for the SEID model is to use at least three base stations to get a high accuracy to further processing of the data. In addition, Koning (2017) and Stierman (2017) also used in one case one dual frequency to create the second frequency for a single frequency receiver using the SEID model.The conclusion of Koning (2017) and Stierman (2017) on this approach is that the accuracy was not high enough to estimate a good zenith wet delay. Furthermore, It is important to keep in mind that the ambiguities of the carrier measurements for both single frequency are not resolved and therefore for every clock reset/cycle slip a new ambiguity appears. Ambiguities must be resolved to get a high precision of the carrier-carrier ionospheric delay. Therefore, no accuracy study is done on this data.

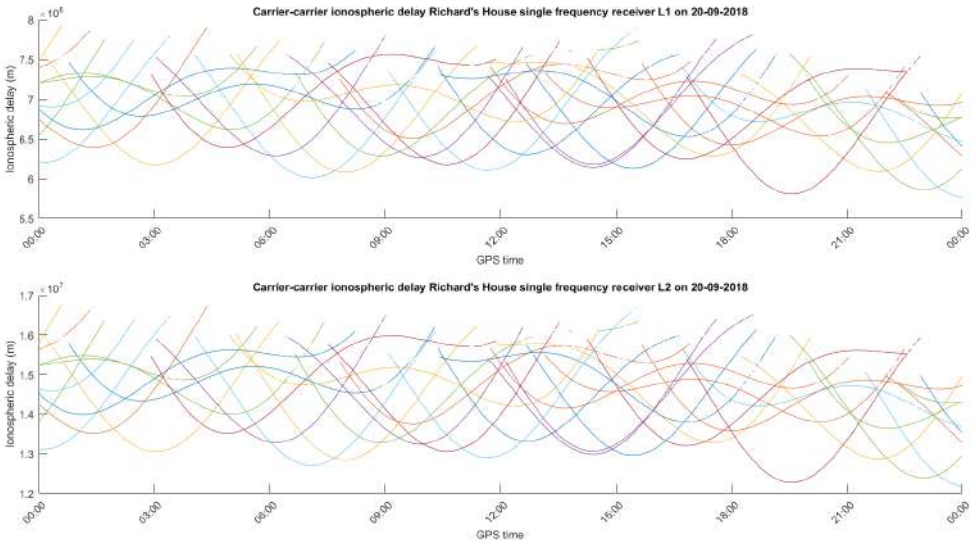

Figure 5.9: Carrier-carrier ionospheric delay of the single frequency receiver at Richard's House. It is important to notice that the y-axis at the top and bottom subplot are not the same. The different colors represent the processed signals received from the different GPS satellites. The figure shows the ionospheric delay for one entire day.

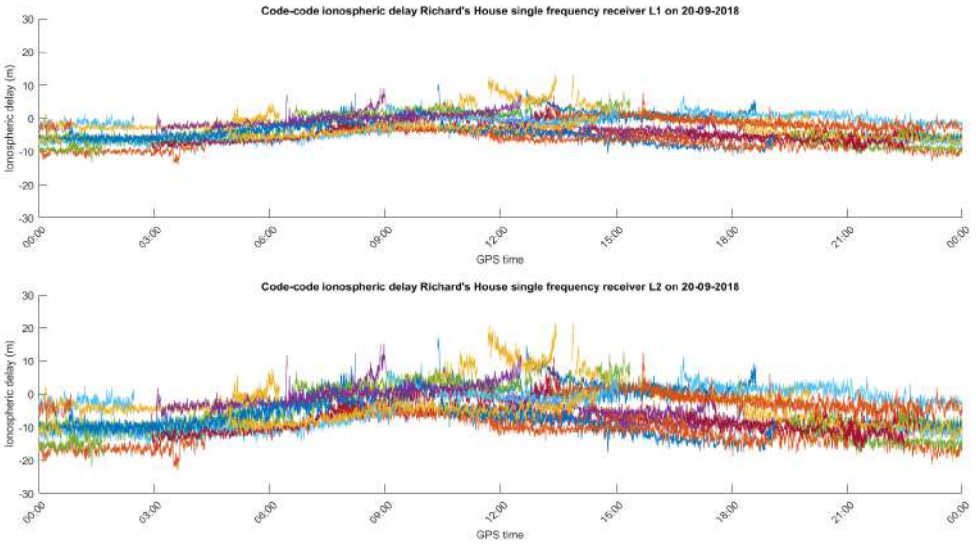

Figure 5.10: Code-code ionospheric delay of the single frequency receiver at Richard's House. The different colors represent the processed signals received from the different GPS satellites. The figure shows the ionospheric delay for one entire day.

5.4. Total electron content

The total electron content is related to the ionospheric delay and it is a way to visualize the spatial variability of the amount of electrons in the ionosphere. Figure 5.11 shows the total electron content at Makerere University, Kampala. For computing the total electron content two approaches are used. Top plot of figure 5.11 shows the total electron content by using the code-code ionospheric delay computed with the ionospheric-free combination. The bottom plot of figure 5.11 is created by using the pseudo-range measurements straightly. For both subplots in figure 5.11 the code measurements are chosen, since they are unambiguous. For the computation of the total electron content the errors are ignored. Looking at figure 5.11 both plots shows the same results. However, the figure shows that the total electron content is sometimes negatively. In theory this is not possible, because the total electron content should be an absolute number (always positive). The errors are even for the dual frequency receiver at Makerere so huge that it gives an negative total electron content. When looking at the behaviour of the signal in figure 5.11, it is visible that the total electron content increases in the morning. This increase corresponds with the expectation that total electron content will increase in the morning because the sun is at the horizon. In the evening there is a clear decrease of the total electron content.

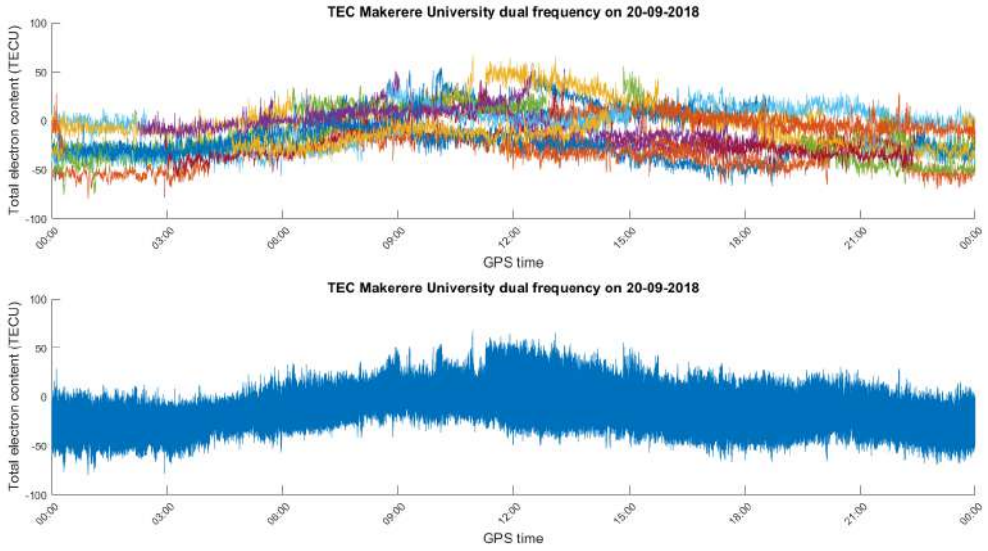

Figure 5.11: Total electron content (TEC) at Makerere University, Kampala using the dual frequency receiver. Top figure uses the ionospheric delay to compute the TEC. Bottom figure is created uses the pseudo range measurements.

6

Conclusion

During this research the behaviour of the ionospheric layer in the atmospheric for one day at the equator in a rainy season is investigated. The main question for this research is :

What accuracy can be obtained for ionospheric delay in Uganda using single and dual frequency receivers and what is the total electron content in the ionosphere?

The main research question is answered using the following sub-questions:

Can the ionospheric delay be determined with single frequency receivers?
In this research the SEID model is tested on the single frequency receiver. When looking at the results the carrier measurements obtained by the u-blox M8T and the corresponding antennas are not accurate enough for estimating the ionospheric delay. The inaccuracy is caused by large multipath errors and cycle slips. The code measurements are not depending on ambiguities, which results in a higher accuracy of the signal compared to the carrier measurements. Due to noise in the signal caused by multipath errors, clock errors and satellite ephemeris error, the ionospheric delay at single frequency receivers can not be determined with the equipment used in this research.

What is the difference in ionospheric delay between single frequency and dual frequency at the same location?
One of the limitation of this research is the limited amount of data received by the single and dual frequency receivers. The failed dual frequency receiver at Ndejje Secondary School is used to create the second frequency for the SF receivers in SEID model. Previous researches recommend to use at least three reference dual frequency station to get a high enough accuracy and reliable observations. Since the dual frequency at Ndejje Secondary School did not work properly, only two working dual frequency receivers are available. Furthermore, looking at the set-up of the single and dual frequency receiver at Richard's house and his neighbours house large multipath errors can occur since receivers are surrounded by buildings and watertank towers. Due to the errors in the signal and the high influence of the dual frequency receiver at Ndejje Secondary School, a clear difference between the estimated ionospheric delay between the SF and DF receivers could not be made with certainty. To investigate the difference in ionospheric delay between SF and DF at the same location the observations should have a higher accuracy.

How does the ionospheric delay and total electron content spatially vary throughout a day?
When looking at the ionospheric delays and the created second frequency of the SF receivers using the SEID model, outliers and cycle slips are visible in the observations. The total electron content can be computed using the pseudo range measurements and the code - code ionospheric delay. For this study only the total electron content is computed by code measurements because code measurements are unambiguous. When computing the total electron content with the code measurements, the daily time serie gives results in negative values for certain moments of a day. In theory, total electron content can not be negative. Since the errors/noise in the computation of the TEC are assumed to be negligible a positive result is assumed. However, in this research with current assumptions this is not happening. Therefore, it can be concluded that the errors/noise are of such a huge influence that the total electron content can not be measured accurately enough. With this conclusion and the lack of data the total electron content can not be quantified. However, there is trend visible, which can be the daily spatial variability of the total electron content. In the morning the total electron content is increasing and in the evening and night the total electron content is decreasing. However, for this study it is important to keep in mind that with only analyzing one day of data conclusions about the variation of the ionospheric delay and the total electron content can not be made. To give a reliable conclusion about the variation of a signal throughout a day multiple days should be analyzed.

As a conclusion on the main question, the accuracy on the ionospheric delay is undetermined because of equipment failure. For this study the computed ionospheric delay of the single frequency receivers are affected by the clock jumps at the dual frequency receiver in Ndejje. Therefore, the multipath error and errors caused by the clock jumps of the computed ionospheric delay are so large that an accuracy study does not give extra information. For further processing a much higher accuracy of the observations are needed. Furthermore, due to these huge errors a realistic estimate of the total electron content in the ionosphere can not be quantified in this study using single frequency receivers. In theory, the total electron content can be a tool to tell when the ionospheric delay will be higher or lower. Looking at the results of the total electron content it can be concluded that the errors occurring in this study are to big to quantify the total electron content. These errors causes a large inaccuracy of the measurements obtained by the single and dual frequency receivers.

7

Recommendations

In this chapter the recommendations for future research are described. The recommendations are split in several sub sections where changes in the research are recommended.

7.1. Network set-up

The setting of the single or dual frequency was far from optimal. The single frequency was most of time situated on a water tank tower, which has an iron structure. This structure can cause an multipath error where the multipath error can be increased by the surrounded roofs at the watertank tower. The multipath error creates more noise in the signal. One of problems facing in the fieldwork was the willingness of school to set-up the equipment. Due to a limited time span, not ideal set-up location were used. Single receivers were set-up at the outer boundaries of the dual frequency area. An unbalanced distributed set-up of the single frequency receiver around the dual frequency receiver has an accuracy effect on generated second frequency of the single frequency receiver. For further research in computing and monitoring the ionospheric delay, TEC content or other atmospheric parameters a network set-up is recommended with equal distributed receivers. To look if the methodology is working with this or similar equipment a fieldwork campaign in the Netherlands would be more easier to organise. The willingness to set-up a GPS receiver is much more likely to be higher than in Uganda and there are less power interruptions. If the results then are promising, then a fieldwork campaign can be advice to set-up. Furthermore, a fieldwork campaign over a longer time, preferably where measurements are collected continuously with an unchanged short time interval, is advised to monitor the changes in ionospheric delay. A fieldwork campaign for at least a year is needed to investigate the seasonal change. To investigate the effect of the solar cycle on the ionospheric delay a fieldwork campaign for at least 11 years is needed.

7.2. Data

One of main problem faces during this research was the lack of data. This is because one of the TRIMBLE dual frequency receivers, which was stationed at Ndejje Secondary School, failed to work. Therefore, for only one measurement day data was available. One of the reason for lacking observation data is that the single frequency receivers track the satellites only for 36 to 57 hours depending supply needed from the powerbanks. This shortage of power supply for the single frequency receivers decreases the time span of the measurements. Furthermore, the long time power interruptions interfere with tracking the signal for the dual frequency signal. This is because when power failure occur, the dual frequency uses the battery of the receiver as power supply. This gives that at short-time power interruptions the TRIMBLE dual frequency receivers logged the GPS signals still but for longer power failure the battery is at one point empty. It is important to know that in theory the estimations of the logged GPS signal will have an higher accuracy, due to decreasing standard deviation, when the equipment has a longer period to measure.

7.3. Data processing

In this research improvements can be made in the data processing. In the research cycle slips and outliers are not removed from the measured data. When removing the outliers and cycle slipe, this can decrease the noise. A better idea to use the data for the dual frequency receiver at Ndejje High School is to delete the cycle slips and outliers and then use an interpolation of the signal in time to fill up the data gaps [Xu, 2016].

7.4. U-blox Dual frequency receivers

When conducting the fieldwork, U-blox only had low-cost single receivers available. However, at the moment of writing this report there are newly available u-blox dual frequency receivers on the market. Therefore, the whole SEID model is not needed to compute and monitor the ionospheric delay, when using the u-blox dual frequency receiver. A recommendation will be to use better antennas. The antennas used in this research are in my opinion not suitable for conducting the same receiver but then with the u-bloc dual frequency receivers. For the ionospheric delay the accuracy of cm can be enough. However, the main aim for the TWIGA project is to compute the water vapour. For that project, when computing the tropospheric delay this is not accurate enough.

7.5. Other models

At this research only SEID model is used and looked at. However, another ionospheric models are available like for example the HiRIM. which is introduced by Rocken et al. (2000). HiRIM generates at every epoch for every satellite an ionospheric correction at a high resolution [Rocken et al., 2000]. The approach is based on the residuals of the double-differenced observations from the surrounding grid of GPS sites and applied to SF stations for even real-time precise positioning [Rocken et al., 2006]. An other way to process a network of dual frequency receivers, which are densified with single frequency receivers, is by using the virtual reference station (VRS) method by Jannsen and Rizos (2005). This VRS method uses measurements from the dual frequency receivers and interpolated to virtual reference station close to a single frequency receiver [Janssen and Rizos, 2005].

In general this research should not be continued in this setting. Future studies should more focus on the power supply to the receivers so that a proper research can be conducted. Currently, the powerbanks are not giving a power supply long enough to obtain reliable results in this study and too much power breaks occur in the electricity network of Uganda. Nowadays, too many secondary problems have occurred that does not benefit this research. They first have to be remedied. In addition, the research will have to be conducted for a longer period of time. With the arrival of the low cost u-blox dual frequency receivers the single frequency receiver are outdated. Using the low-cost u-blox dual frequency receivers the ionospheric delay can be estimated directly from the measurements. The GPS networks can be more densified using the u-blox dual frequency receivers to capture the high spatial variability of the water vapor and total zenith delay. However, it is important to keep in mind that the ionospheric will still be the biggest error source in the GPS signal. Lastly, to set-up an ideal network. so the multipath error will be significantly reduced, will still be a big obstacle to overcome. The receiver should have a clear view of the sky and should be set-up in an area where low multipath errors occur. It is very difficult to find and gain access to such a spot in an urban area as Kampala.

Bibliography

[Abba et al., 2015] Abba, I., Abidin, W., Masri, T., Ping, K., Muhammad, M., and Pai, B. (2015). Ionospheric effects on gps signal in low-latitude region: a case study review of south east asia and africa. *Nigerian Journal of Technology*, 34(3):523–529.

[Bender et al., 2011] Bender, M., Dick, G., Ge, M., Deng, Z., Wickert, J., Kahle, H.-G., Raabe, A., and Tetzlaff, G. (2011). Development of a gnss water vapour tomography system using algebraic reconstruction techniques. *Advances in Space Research*, 47(10):1704–1720.

[Braun et al., 1999] Braun, J., Rocken, C., Meertens, C., and Ware, R. (1999). Development of a water vapor tomography system using low cost l1 gps receivers.

[Deng et al., 2009] Deng, Z., Bender, M., Dick, G., Ge, M., Wickert, J., Ramatschi, M., and Zou, X. (2009). Retrieving tropospheric delays from gps networks densified with single frequency receivers. *Geophysical Research Letters*, 36(19).

[Deng et al., 2011] Deng, Z., Bender, M., Zus, F., Ge, M., Dick, G., Ramatschi, M., Wickert, J., Löhnert, U., and Schön, S. (2011). Validation of tropospheric slant path delays derived from single and dual frequency gps receivers. *Radio Science*, 46(06):1–11.

[Deng et al., 2012] Deng, Z., Bender, M., Zus, F., Ge, M., Dick, G., Wickert, J., and Schon, S. (2012). Gps meteorology with single frequency receivers.

[Guo et al., 2015] Guo, J., Li, W., Liu, X., Kong, Q., Zhao, C., and Guo, B. (2015). Temporal-spatial variation of global gps-derived total electron content, 1999–2013. *PLOS ONE*, 10(7):1–21.

[Janssen and Rizos, 2005] Janssen, V. and Rizos, C. (2005). Mixed-mode gps deformation monitoring—a cost-effective and accurate alternative? In *A Window on the Future of Geodesy*, pages 533–537. Springer.

[Koning, 2017] Koning, A. (2017). Precipitable water vapour estimation using gps in uganda: A study on obtaining the zenith wet delay. http://resolver.tudelft.nl/uuid:ec036b6b-b914-4b53-95f8-63638a0faa10.

[Krietemeyer et al., 2018] Krietemeyer, A., ten Veldhuis, M.-c., van der Marel, H., Realini, E., van de Giesen, N., et al. (2018). Potential of cost-efficient single frequency gnss receivers for water vapor monitoring. *Remote Sensing*, 10(9):1493.

[Li et al., 2018] Li, H., Liao, X., Li, B., and Yang, L. (2018). Modeling of the gps satellite clock error and its performance evaluation in precise point positioning. *Advances in Space Research*, 62(4):845–854.

[Misra and Enge, 2001] Misra, P. and Enge, P. (2001). Global positioing system: Signals, measurements, and performance.

[Natural Resources Canada, 2019] Natural Resources Canada (2019). Tools and applications. https://www.nrcan.gc.ca/maps-tools-publications/tools/geodetic-reference-systems-tools/tools-applications/.

[Poh and Kamarudin, 2006] Poh, O. H. and Kamarudin, M. N. (2006). Calculation in estimating total electron gps. http://eprints.utm.my/.

[Rocken et al., 2000] Rocken, C., Braun, J., VanHove, T., and Ware, R. (2000). Gps networks for atmospheric sensing. Proceedings of the ION National Technical Meeting.

[Rocken et al., 2006] Rocken, C., Lukes, Z., Mervart, L., Johnson, J., Iwabuchi, T., and Kanzaki, M. (2006). Real-time ionospheric and atmospheric corrections for wide area single frequency carrier phase ambiguity resolution. In *Proc. ION-GNSS 19th Intl. Technical Meeting of the Satellite Division, Inst. of Navigation, Fort Worth, Texas*, volume 12081218.

[Royal Observatory of Belgium GNSS Research Group, 2014] Royal Observatory of Belgium GNSS Research Group (2014). Ionosphere tutorial. http://www.gnss.be.

[Stierman, 2017] Stierman, E. (2017). Precipitable water vapour estimation using gps in uganda: Measuring and modelling the precipitable water vapour using single and dual frequency gps receivers. http://resolver.tudelft.nl/uuid:05c87122-00a5-4b3b-937a-10bc76078a9a.

[TAHMO, 2020] TAHMO (2020). About tahmo. https://tahmo.org/.

[Teunissen and Montenbruck, 2017] Teunissen, P. and Montenbruck, O. (2017). Springer handbook of global navigation satellite system. https://www.springer.com/gp/book/9783319429267.

[TU Delft, 2017] TU Delft (2017). H2020 grant for twiga. https://www.tudelft.nl/en/2017/citg/facultair/h2020-grant-for-twiga/.

[TWIGA, 2020] TWIGA (2020). Transforming water, weather, and climate information through in situ observations for geo-services in africa. http://twiga-h2020.eu/index.html.

[Van Sickle, 2017] Van Sickle, J. (2017). cycle slip. https://www.e-education.psu.edu/geog862/node/1728.

[Williams, 2001] Williams, J. (2001). The global positioning system - background/overview. http://www.ae.utexas.edu/courses/ase389p7/projects/williams/background.html.

[Xu, 2016] Xu, C. (2016). Reconstruction of gappy gps coordinate time series using empirical orthogonal functions. *Journal of Geophysical Research: Solid Earth*, 121(12):9020–9033.

[Zumberge et al., 1997] Zumberge, J., Heflin, M., Jefferson, D., Watkins, M., and Webb, F. H. (1997). Precise point positioning for the efficient and robust analysis of gps data from large networks. *Journal of geophysical research: solid earth*, 102(B3):5005–5017.

Appendices

A

Data conversion

A.1. Dual frequency

The dual frequency measurements are saved as a daily file on the SD card in a .t01 format. To process the dual frequency receivers the files are first converted to .180 files using the program Convert To RINEX, version 3.0.7.0. After that the rinex files is send to NRCAN for Precise Point Positioning.

A.2. Single frequency

The single frequency measurements are saved as a hourly file on the SD card in an ubx format. Before processing the single frequency file the ubx files has to be converted to .18o files using the following bat file, which call the teqc.exe programm:

*call teqc -O.o KBeenen -O.ag TUDelft -O.rt U-BLOXM8T -O.at ublox -O.mo ubx0 -O.px X Y Z +obs + +nav +,+ -tbin 1d ubx0 *.ubx*

For every single frequency, the X, Y, Z should be replaced with the Cartesian coordinates of the single frequency receiver. Like for example, the bat code for the single frequency receiver at Onwards & Upwards will be:

*call teqc -O.o KBeenen -O.ag TUDelft -O.rt U-BLOXM8T -O.at ublox -O.mo ubx0 -O.px 5374910.531389905 30366.11404448636 3420388.235079714 +obs + +nav +,+ -tbin 1d ubx0 *.ubx*

Secondly, every Sunday the first data entry in the ubx file is compromised. Therefore, the first epoch should be removed manually and the meta header should be adjusted. The original code to call teqc is written by Andreas Krietemeyer, but adjusted for this research by KBeenen.

B

Ionospheric delay Buloba dual frequency receiver

Using the ionospheric-free combination the ionospheric delay for the code-code and carrier-carrier at Buloba are computed.

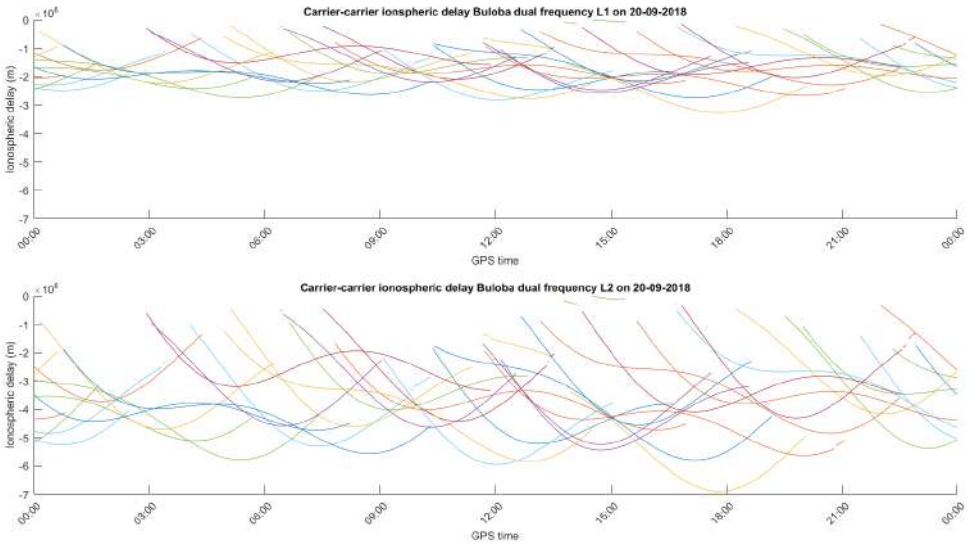

Figure B.1: Code-code ionospheric delay measurement for the dual frequency receiver at Richard neighbours house in Buloba

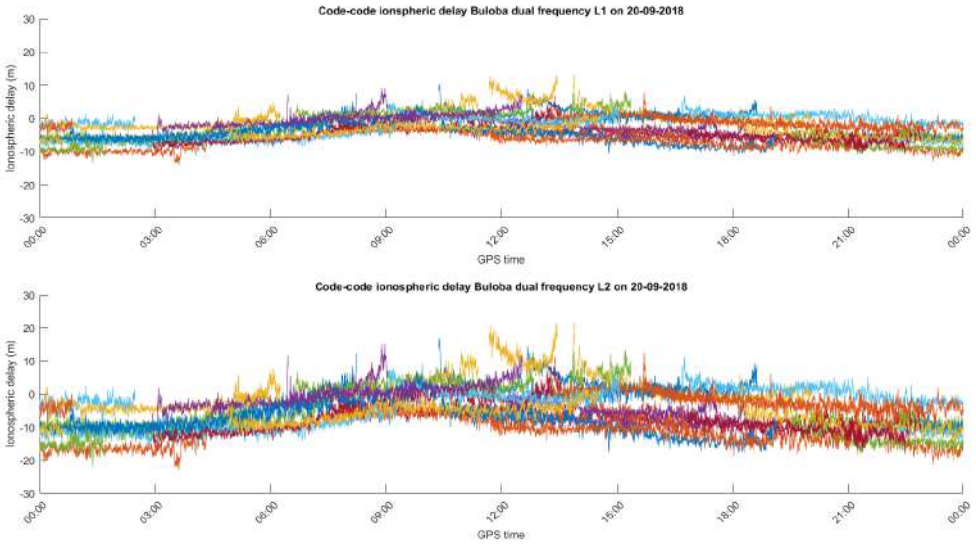

Figure B.2: Code-code ionospheric delay measurement for the dual frequency receiver at Richard neighbours house in Buloba

C

Epoch-difference ionospheric delay

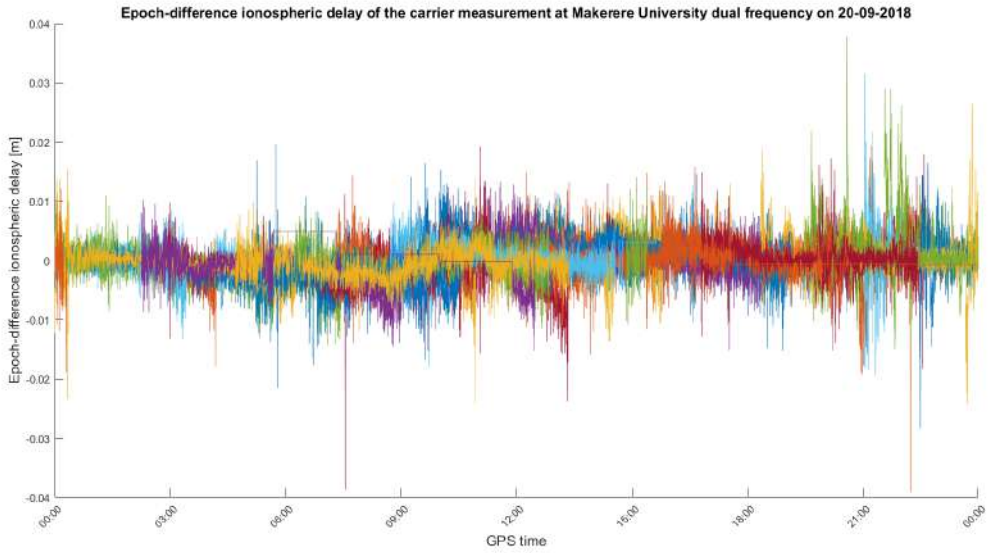

Figure C.1: Epoch-difference ionospheric delay at at Makerere Univeristy, Kampala